



A Quasi-Equilibrium
Kinetic Model of HF Air Breakdown

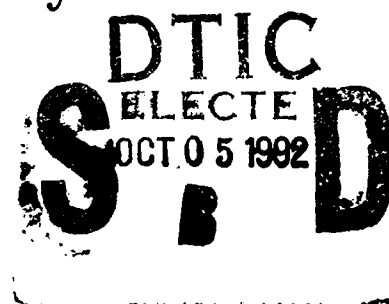
Phase I Final Report
Contract # DAAL02-91-C-0025

Submitted to
Harry Diamond Laboratory

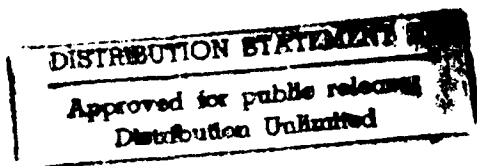
September 1991

by

A. E. Rodríguez and M. G. White



Tetra Corporation
3701 Hawkins St, NE
Albuquerque, NM 87109
(505) 345-8623



02 7 11

396350

92-26362



REPORT DOCUMENTATION PAGE

Form Approved
OMB No. 0704-0188

Public reporting burden for this collection of information is estimated to average 1 hour per response, including the time for reviewing instructions, searching existing data sources, gathering and reviewing the data needed, and completing and reviewing the collection of information. Send comments regarding this burden estimate or any other aspect of this collection of information, including suggestions for reducing this burden, to Washington Headquarters Services, Directorate for Information Operations and Reports, 1215 Jefferson Davis Highway, Suite 1204, Arlington, VA 22202-4302, and to the Office of Management and Budget, Paperwork Reduction Project (0704-0188), Washington, DC 20503.

1. AGENCY USE ONLY (Leave blank)	2. REPORT DATE 9/91	3. REPORT TYPE AND DATES COVERED Final Report 2/91 - 9/91	
4. TITLE AND SUBTITLE A Quasi-Equilibrium Kinetic Model of HF Air Breakdown		5. FUNDING NUMBERS	
6. AUTHOR(S) A. E. Rodriguez and M. G. White		8. PERFORMING ORGANIZATION REPORT NUMBER TR91-17	
7. PERFORMING ORGANIZATION NAME(S) AND ADDRESS(ES) Tetra Corporation 3701 Hawkins Street NE Albuquerque, NM 87109		10. SPONSORING/MONITORING AGENCY REPORT NUMBER	
9. SPONSORING/MONITORING AGENCY NAME(S) AND ADDRESS(ES) Harry Diamond Laboratories 2800 Powder Mill Road Adelphi, MD 20783		11. SUPPLEMENTARY NOTES	
12a. DISTRIBUTION/AVAILABILITY STATEMENT		12b. DISTRIBUTION CODE	
13. ABSTRACT (<i>Maximum 200 words</i>) <p>In Phase I of the program, we developed the basic tools needed to build a high-frequency air breakdown model. We developed a Quasi-Equilibrium Methodology (QEM) for extending fluid electron transport models to the nonequilibrium regime, based on assuming that the transport coefficients relax toward their equilibrium values on time scales quantified by time-dependent Boltzmann equation solutions. Our analysis of nonequilibrium electron transport discovered and explained a velocity overshoot effect that is not generally known. That tendency of the electrons to overshoot the equilibrium drift velocity is shown to have a profound effect on streamer behavior. We examined the extent of possible simplifications to our kinetic air breakdown model, concluding that factors of 2 to 5 speed-up are possible. We have identified the major phenomenological</p>			
14. SUBJECT TERMS dielectric breakdown, kinetics, Boltzmann equation, non-equilibrium transport, streamers, spark, arc, HF discharge		15. NUMBER OF PAGES	
17. SECURITY CLASSIFICATION OF REPORT UNCLASSIFIED		16. PRICE CODE	
18. SECURITY CLASSIFICATION OF THIS PAGE UNCLASSIFIED	19. SECURITY CLASSIFICATION OF ABSTRACT UNCLASSIFIED	20. LIMITATION OF ABSTRACT UNLIMITED	

CLASSIFIED BY:

DECLASSIFY ON:

issues in a modeling strategy, and examined nonequilibrium effects on ionization waves. Finally, we present a plan to complete development of a computational model of High Frequency air breakdown suitable for incorporation into EMP coupling codes, including model verification experiments and implementation of the computer module in an existing EMP coupling code.

Acknowledgements:

We wish to thank several individuals who contributed in various ways to the research reported here. Dr. Chris B. Wallace of BDM International contributed materially to our Phase II Program Plan, identifying many of the code interface issues that will need to be addressed. Dr. Mark J. Kushner of the University of Illinois contributed Appendix B and many useful discussions of modeling issues. Dr. Kambiz Salari provided much needed guidance on numerical issues, especially pertaining to streamer modeling. Dr. W. L. (Skip) Morgan provided invaluable guidance for the modifications of his ELENDF Boltzmann solver. Many others took time for discussions on specific issues, such as Bill Prather of the AFWL, Dr. Fred Blottner of Sandia National Laboratories, Dr. Bernie Penetrante of Lawrence Livermore National Laboratories, Dr. Erik E. Kunhardt of Polytechnic's Webber Research Institute, and Dr. Alan C. Hindmarsh of Lawrence Livermore National Laboratories. We readily acknowledge our indebtedness to all.

DTIC GRA&I

Accession For	
NTIS GRA&I	<input checked="" type="checkbox"/>
DTIC TAB	<input type="checkbox"/>
Unannounced	<input type="checkbox"/>
Justification	
By <i>perform SO</i>	
Distribution/	
Availability Codes*	
Dist	Avail and/or Special
<i>A-1</i>	

TABLE OF CONTENTS

	Page
I. INTRODUCTION.	1
A. Background.	1
B. Phase I Objectives.	2
C. Overview	3
II. NON-EQUILIBRIUM ELECTRON TRANSPORT	6
III. TIME-DEPENDENT BOLTZMANN ANALYSIS OF KINETIC RELAXATION.	17
IV. NON-EQUILIBRIUM EFFECTS ON STREAMER PROPAGATION.	28
V. SIMPLIFICATION OF THE AIR BREAKDOWN KINETICS MODEL.	35
VI. TOWARD A HAIRLINE APERTURE BREAKDOWN MODEL.	43
VII. PHASE II PROGRAM PLAN.	49
A. Phase II Technical Objectives.	49
B. Phase II Work Plan.	50
VIII. SUMMARY AND CONCLUSIONS.	62
REFERENCES	64
APPENDIX A	A-1
APPENDIX B	B-1

A Quasi-Equilibrium Kinetic Model of HF Air Breakdown

I. INTRODUCTION.

A. BACKGROUND.

This project was initiated with the express purpose of developing a model of air breakdown in apertures subjected to high-frequency (HF) electromagnetic pulses. High-altitude electromagnetic pulse (HEMP) threat levels and frequency content are determined primarily by the device rise time, and for nominal parameters, are in the regime of 30 kV/m with significant energy content up to 10's of MHz [Ref. 1]. The requirement for the project was inspired by the observation of ubiquitous shot-to-shot variations in the response of shielded systems to EMP in simulation experiments, leading to the hypothesis that air breakdown was occurring in the seams of apertures. Methods to solve the field distributions near an aperture are well known, at least in the linear regime before the air breakdown. The challenge is to correctly model the highly nonlinear breakdown processes for an EMP-like driving field pulse. Because of the nonlinearity of the reactions, a time-domain approach is needed. However, because the time regimes of interest, though less than the closing times, are slow compared to electron collision frequencies, an equilibrium or quasi-equilibrium kinetic treatment is possible.

We have recently built a kinetic model of air breakdown capable of predicting spark gap closing times τ_c for a both over- and under-volted spark gaps [Ref. 2]. The closing time is determined primarily by ohmic heating which eventually enables thermal ionization to take over. EMP pulse-widths may be long enough to permit sufficient ohmic heating to cause breakdown. We have found that under-volted gap closure is explained by electron detachment from O^- . Simulated closing times agree with empirical data in a range from 10 × over-volted to 10 × under-volted, which varies approximately as:

$$\rho\tau_c = 7.4 \times 10^{14} (E/\rho)^{-3.44}$$

[Ref. 3] where $\rho = 1.29 \text{ kg/m}^3$ in 1 atm air, and E is in V/m.

We set out to build a quasi-equilibrium kinetic model of HF air breakdown based

on our spark breakdown model. An understanding of the time-dependent breakdown process is the most critical prerequisite to building a complete phenomenological model of HF arcing in apertures illuminated by EMP. The EMP energy leaking through an aperture will depend primarily on how long it takes for the arc to form (~100 ns); and to a lesser degree on how well the arc plasma shields against further energy transfer after it is well-formed. Furthermore, the fast collapse of the voltage across the aperture can create very high frequency noise inside the shielded enclosure, thus actually enhancing the high-frequency content of the transferred EMP. The Phase I program reduced this highest risk factor by examining the critical phenomenology first, and demonstrating the adequacy of an innovative modeling methodology to model HF breakdown processes.

B. PHASE I OBJECTIVES.

The ultimate goal is to develop and verify a self-consistent theoretical model of air breakdown in apertures illuminated by EMP. That goal was supported by the following Phase I objectives:

1. Determine streamer behavior in feasible E-pulse profiles. Key output parameters are the speed of propagation and nominal electron density created by a streamer.
2. Determine the adequacy of a quasi-equilibrium kinetic model. Key parameters are the characteristic times for reaching equilibrium values of ionization, attachment and other kinetic rates, as they compare to pulse-width.
3. Plan for complete model development. Phase I 0-D and 1-D models would uncover physics and numerical issues that will be more challenging in higher dimensions. We would determine the appropriate dimensionality (1-D, 2-D or 3-D), and develop a plan for developing such a model in Phase II.
4. Plan for experimental verification. Phase I analysis would identify uncertainties in the model. We would develop detailed plans to remove or reduce the most significant uncertainties with experiments which can be performed within the scope of Phase II.

Those objectives were supported by five technical tasks:

1. Boltzmann Analysis. We used a fully time-dependent numerical solution of the Boltzmann operation to quantify the relaxation times of the electron transport coefficients.
2. Streamer Modeling. We implemented the Quasi-Equilibrium Methodology (QEM) in a single 1-dimensional electric field solving code (ELF1D) to determine the effect of QEM on streamer propagation.
3. Kinetic Modeling. We analyzed the significant physics dominating breakdown times in a 0-dimensional kinetics code to determine feasible simplifications.
4. Advanced Model Plan. We identified the dominant phenomenology, and included a complete plan for developing a self-consistent breakdown model in a Phase II Program Plan.
5. Experimental Verification Plan. We included a detailed plan for a Phase II experiment to verify the Phase II model in the Phase II Program Plan.

C. OVERVIEW.

Two main issues were examined in Phase I. The first issue is non-equilibrium transport; the second is the breakdown kinetics.

A clear phenomenological description of the electrical breakdown of high-pressure gaseous insulators has emerged only in the last decade or so. Typically a micro-irregularity (accidental or intentionally triggered) will create a sufficient local disturbance to launch a streamer. By "streamer" we mean a glowing ionization wave which enhances the E-field ahead of its tip, creating intense local excitation and ionization (about 10^{14} e/cm³). Streamers are usually filamentary, because the wave velocity (up to 10^9 cm/s) increases with decreasing radius of curvature, making the tip self-sharpening. Once the filamentary streamer connects to the other electrode, the partially ionized filament draws current; not enough to cause voltage collapse for reasonably large circuit capacitance, but enough to cause

significant ohmic heating. When the filament temperature exceeds about 10,000 K, thermal ionization dominates. At that point, the system becomes strongly non-linear, because the higher the temperature, the faster the thermal ionization; the higher the ionization, the faster the ohmic heating. The rapidly rising current causes sudden voltage collapse, and the filamentary glow discharge then quickly evolves into an arc.

We recognized that the fast streamer time scales (significant changes in local E-field and electron density in a few picoseconds) were comparable to collision frequencies (a few per ps). Therefore, equilibrium fluid transport techniques are questionable. However, since the deviation from equilibrium are not likely to be very great, a perturbation method may adequately model this quasi-equilibrium regime. This would avoid expensive particle-pushing techniques (e.g. Monte-Carlo), which are more appropriate when the transport is nearly ballistic (collisionless) than when it's collision-dominated. Thus, the objective of our Quasi-Equilibrium Methodology was to extend fluid model techniques with first-order non-equilibrium effects.

Filamentary streamers may not form in the small micro-gaps in the apertures of EMP-hardened structures, because their sizes are comparable to expected streamer diameters. However, the electrons emitted from a cathode are never in equilibrium with the local electric field in the gas, and the disturbance due to the discontinuities in E-field, and the density, initial velocity and mean energy of the injected electrons take a certain distance to relax to equilibrium in the gas interior. This disturbance, which persists in steady-state, is known as a cathode fall. Viewed from the perspective of a fluid "particle" (a clump of electrons), the cathode boundary conditions are exactly analogous to temporal initial conditions. Whether the cathode fall in a micro-gap with increasing voltage evolves into a Townsend avalanche or an ionization wave (planar or filamentary), it is clear that non-equilibrium effects must be considered. Our Quasi-Equilibrium Methodology (QEM) emphasizes the temporal approach.

Our methodology (QEM) is based on assuming that the transport coefficients relax toward their equilibrium values on quantifiable time scales. The implications of non-equilibrium effects are examined in detail based on order-of-magnitude estimates in Chapter II. One interesting consequence is an electron velocity over-

shoot for sudden E-field changes, which can significantly affect streamer propagation. The quantification of relaxation times based on time-dependent Boltzmann equation solutions is described in detail in Chapter III. The main conclusion is that the transport coefficients relax on time scales comparable to the energy transfer time. The non-equilibrium effects are important in modeling fast streamers or planar ionization waves which trigger the breakdown process, or in modeling the cathode fall or Townsend avalanche steady-state which defines initial conditions for the kinetic breakdown model. The effect on streamer propagation is shown in Chapter IV.

The breakdown process itself occurs on a time scale long compared to relaxation times. Chapter V describes our assessment of the potential to simplify the full kinetic model of air breakdown, in order to make it practical for 1-dimensional or multi-dimensional codes. The main conclusion is that factors of 2 to 3 in computational speed can be gained. Chapter VI discusses various issues involved in developing a modeling strategy. It develops in detail the rationale for our phenomenological approach for Phase II.

The modeling approach is included in the Phase II Program Plan, which constitutes Chapter VII. It includes the model development proper, validation procedures, and implementation in an existing EMP coupling code. The validation includes the verification experiment plan. The demonstration EMP code is the POLYANA code developed by BDM, and will require their participation in Phase II. Phase III will include marketing of the QEM module as a stand-alone product.

Appendices cover two esoteric topics. Appendix A describes the derivation of the Relaxation to a Sliding Quasi-Equilibrium (RSQE) algorithm which makes the QEM approach computationally affordable. Appendix B considers the effect of dust particles on the kinetics and transport, and demonstrates it can be neglected.

II. NON-EQUILIBRIUM ELECTRON TRANSPORT.

The key to the Quasi-Equilibrium Methodology (QEM) is the time-dependent Boltzmann equation solution. However, some of the expected behavior can be examined with order-of-magnitude estimates based on reasonable assumptions and approximations. This chapter examines the expected non-equilibrium electron transport behavior, specifically electron velocity and electron multiplication.

Since the momentum transfer process is dominated by the lower energies in the electron energy distribution function (EEDF), we should expect the relaxation of the momentum transfer collision frequency to occur on the same time scale as energy transfer. An estimate of the energy transfer time can be obtained as follows. At equilibrium, the energy losses must equal the gains from ohmic heating. Therefore, the energy transfer time is the ratio of mean electron energy $\langle \mathcal{E} \rangle$ to the ohmic heating rate. For 3 MV/m in 1 atm air, the mean electron energy is about 3 eV. Thus, the relaxation time is about

$$\tau \approx \frac{\langle \mathcal{E} \rangle}{e E V_d} \approx 10^{-11} \text{s}$$

where e is the elementary charge. In comparison, the equilibrium drift velocity, V_d , for a nominal $E = 3$ MV/m in 1 atm air is about 10^5 m/s. Thus, the momentum transfer collision frequency is about

$$\nu = \frac{e E}{m V_d} \approx 5 \times 10^{12} / \text{s}$$

where m is the electron mass. Therefore, we should expect the momentum transfer relaxation time τ to be about 50 collision times ($1/\nu$).

To illustrate what this means, consider a homogeneous E-field turned on "instantaneously" (fast compared to the collision frequency). Neglecting spatial terms, this is an initial-value problem, requiring integration only in time. Before the step, all values are in equilibrium for $E = 0$. The initial velocity is 0, but the initial collision frequency is not 0, because random motion produces collisions even without an E-field. From low air mobility data [Ref. 4] we can assume an initial value $\nu(0) \approx 1/\text{ps}$ (vs the equilibrium value $\nu_q = 5/\text{ps}$). With those

conditions, we solved the Ordinary Differential Equation (ODE) pair

$$\dot{V} = \frac{e}{m} E - V \nu \quad \text{and} \quad \dot{\nu} = (\nu_q - \nu) / \tau$$

for time-dependent (non-equilibrium) electron velocity, V , and collision frequency, ν , by the Relaxation to a Sliding Quasi-Equilibrium (RSQE) method [Appendix A]. Figure 1 shows the collision frequency relaxing toward the equilibrium value of 5/ps. Notice there is still a significant gap after 10 ps, which is one relaxation time τ . Figure 2 shows the behavior of the electron velocity. Notice V relaxes to the Sliding Quasi-Equilibrium (SQE) curve much faster than the SQE relaxes to the eventual equilibrium drift velocity V_d . The test case conditions instantaneously increase the driving term E , but the drag-inducing collision frequency, ν , increases much more slowly. The result is that the electron fluid velocity overshoots the equilibrium value V_d and then relaxes toward it from the high side on the energy transfer time scale.

This phenomenon can have a profound effect on the behavior of the streamer propagation model and a non-equilibrium cathode fall model. The tendency of the electron fluid to "over-react" to the sudden change in E -field will make the streamer tip sharper (more shock-like), and may explain why streamer models based on equilibrium transport generally underestimate the streamer propagation velocity. Consider that the integral of the electron velocity is a total displacement, and the charge separation is what distorts the field at an ionization wave-front. The total displacement $\int V dt$ computed by the RSQE method out to several τ -values is about 1.4×10^{-6} m more than using the equilibrium V_d . For a nominal 10^{20} e/m³ (10^{14} /cm³), such an error in charge separation will translate into an error in computed space-charge field of

$$\delta E = \delta X e N_e / \epsilon_0 \approx 2.6 \text{ MV/m}$$

where N_e is electron density, and ϵ_0 is the permittivity of free space. That is not a negligible effect, even though the "overshoot" occurs on a time-scale of about 10 ps.

A reasonable upper bound for both an ionization wave-front and for a typical

cathode fall (CF) in 1 atm air is about 10 MV/m. For that field, the drift velocity increases to about 2×10^5 m/s, leaving the collision frequency about the same as assumed above for 3 MV/m. Furthermore, the mean energy increases to about 5 eV, leaving the energy transfer time about the same. Therefore, the relaxation time scales of the above analysis are insensitive to E-field, although the equilibrium drift velocity V_d increases approximately in proportion to E. The total displacement error δX if non-equilibrium effects are ignored estimated above for 3 MV/m would double (proportional to V_d) for 10 MV/m, and so would the resulting space-charge field error estimate δE .

The effect of non-equilibrium ionization is harder to evaluate. The field distribution in both an ionization wave and a cathode fall is dominated by the space-charge effect, and that is dominated by the electron multiplication (given by the ionization rate coefficient). The ionization rate is dominated by the high-energy tail of the EEDF, which is expected to relax on a slower time scale than the mean energy. For 10 MV/m in 1 atm air, the equilibrium ionization rate ν_i is about 3×10^9 /s. This leads to CF scale-size estimates in the regime of 10^{-4} m (10^{-2} cm), which is comparable to the expected micro-crack sizes. However, the electron emission mechanisms are unlikely to produce electrons above the ionization thresholds (>12 eV), but will produce plenty above the dissociative attachment threshold (~ 3 eV). Therefore, the appropriate initial (boundary condition) ionization rate $\nu_i(0)$ is much smaller than the attachment rate $\nu_a(0)$, which will be close to its equilibrium value of about 10^8 /s. If the ionization rate relaxation time is much slower than $1/\nu_i$, the electron multiplication in a sub-mm aperture will be much less than calculated by equilibrium models.

For illustrative purposes, we solved the ODE pair

$$\dot{N}_e = S - N_e(\nu_a - \nu_i) \quad \text{and} \quad \dot{\nu}_i = (\nu_q - \nu_i)/\tau_i$$

with the initial conditions $N_e(0) = 10^5/\text{cm}^3$ and $\nu_i(0) = 0$, a constant equilibrium ionization rate $\nu_q = 3/\text{ns}$, and relaxation time τ_i varying from 0.1 to 3.0 ns. The background source S was chosen so the pre-existing steady-state value S/ν_a matched the initial electron density $N_e(0)$. The ionization rate grows quickly, so the net $(\nu_a - \nu_i)$ becomes a gain (multiplication) term almost immediately.

Figure 3 shows the relaxation of the net gain rate ($\nu_i - \nu_a$), which is positive ($\nu_i > \nu_a$) most of the time. Figure 4 shows the resulting electron multiplication curves. Note that on a log-linear plot, positive slope corresponds to net gain multiplication rate ($\nu_i - \nu_a$). The $\tau_i = 0.1$ ns curve is almost an equilibrium solution, which assumes the ionization rate ν_i comes into equilibrium with the E-field virtually instantaneously. The value of the relaxation time τ_i clearly can affect the order of magnitude of the electron number density in a hairline crack created by an overvoltage, and must be evaluated for the QEM approach.

This test case is analogous to a cathode fall, but only roughly. In a real cathode fall [Ref. 5, 6, and 7], the E-field drops off approximately linearly, but a nominal 10 MV/m is the right order of magnitude. The analogous test case we constructed corresponds to a constant 10 MV/m, and since the drift velocity relaxes to the equilibrium 2×10^5 m/s on a 10-ps time scale, 5 ns in time roughly corresponds to 1 mm in distance.

However, the E-field is not going to be constant, either in a CF or a micro-crack. Assuming sharp edges enhance the peak field, since the equilibrium ionization rate is very sensitive to E-field, it is not unrealistic to assume the equilibrium rate ν_i starts at about 10/ns, but decreases to much less than the nominal 3/ns. Therefore, we repeated the CF-analogue analysis with the equilibrium ν_i decreasing from 10 to 0.3 /ns. Figure 5 shows the resulting instantaneous ionization rates curves. The increase for slower τ_i at late times reflects the fact that slower relaxation times delay the cooling of the high-energy tail of the EEDF as much as its heating at early times. Figure 6 shows the resulting electron multiplication curves. Notice the lower- τ_i curves eventually exceed $10^{14}/\text{cm}^3$. Near those levels, streamer-like ionization waves may form and ionize the whole gap.

For 0.1-mm micro-gaps, the avalanche discharge would be truncated at a position corresponding to about 0.5 ns. However, the effective heating and electron multiplication would accumulate for a sinusoidal driving signal from one half-cycle to the next. To first order, each 0.5-ns interval represents a half-cycle. Considering that the polarity changes every half-cycle, the new cathode initial conditions are the previous half-cycle's final conditions at the anode. If we assume breakdown occurs in the cycle where N_e reaches $10^{14}/\text{cm}^3$, we conclude

that several cycles will be needed.

Non-equilibrium effects on the electron multiplication will be negligible if the ionization coefficient relaxation time τ_i is slow compared to the multiplication time $1/\nu_i$, but will dominate if $\tau_i > 1/\nu_i$. The time-dependent Boltzmann analysis leads to quantitative estimates of all relaxation times.

Non-Eq. Momentum Transfer Coll. Frq.

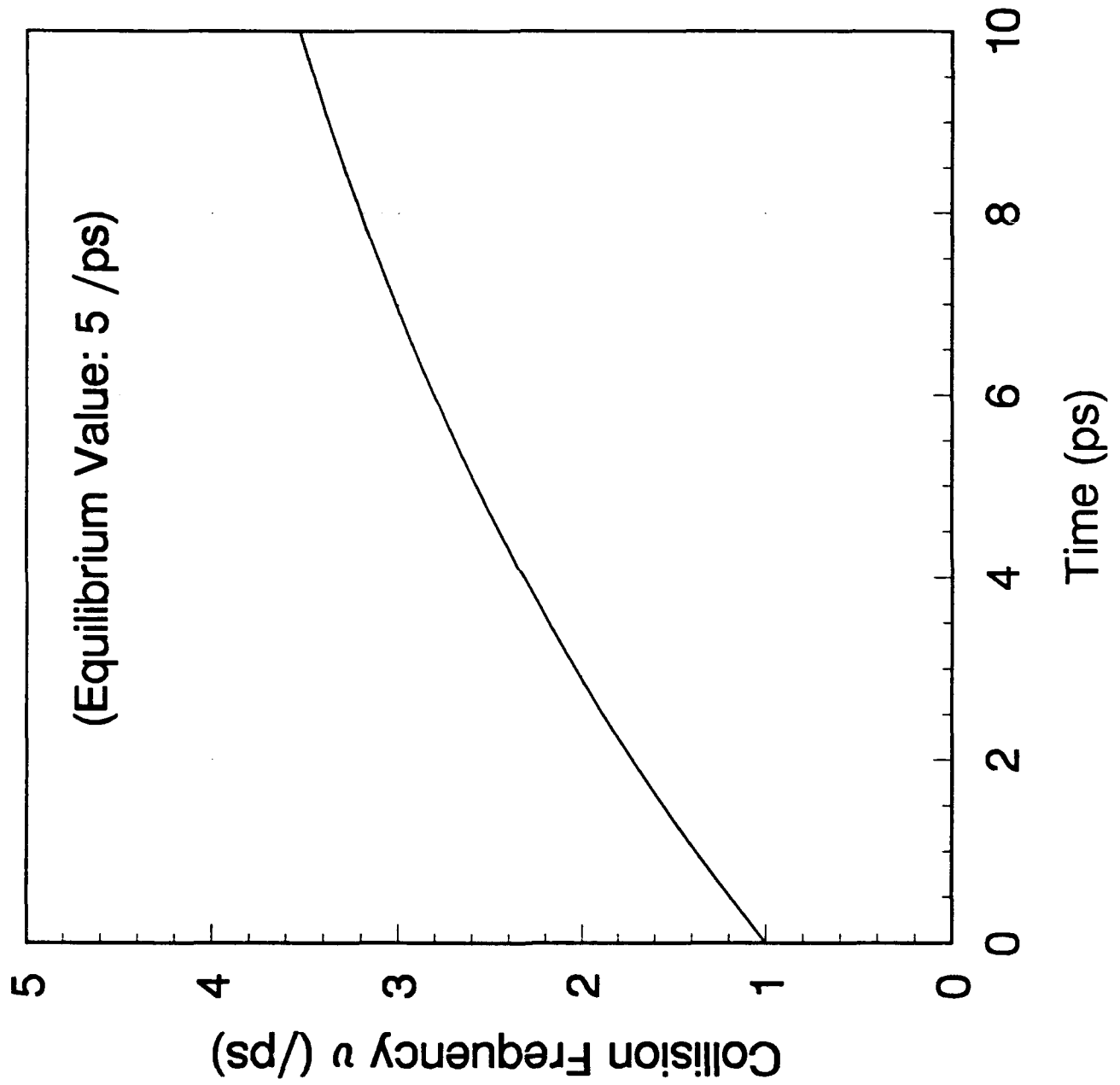


Figure 1. Relaxation of ν : 1/ps \rightarrow 5/ps in 10 ps.

Non-Equilibrium Electron Velocity

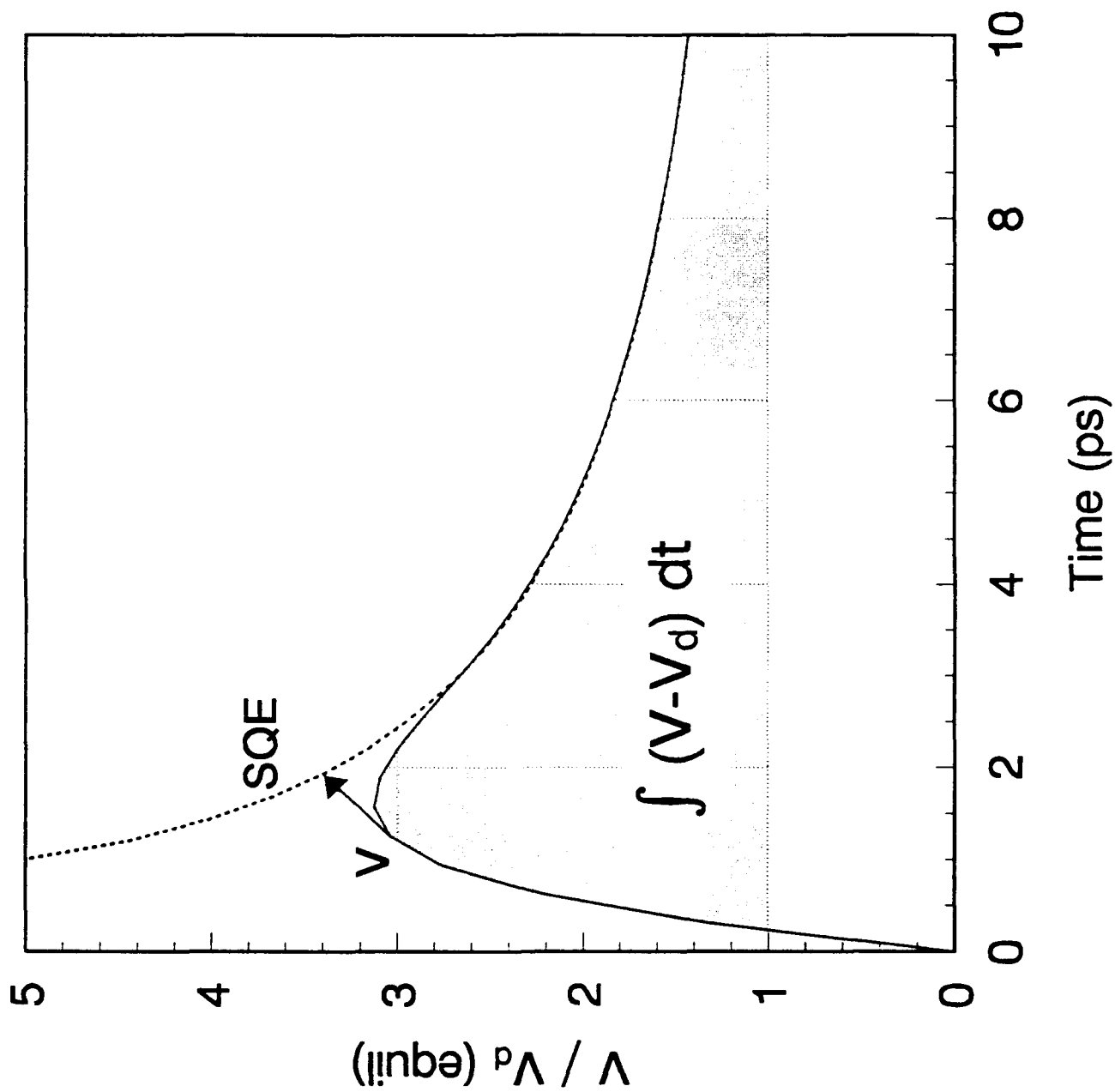


Figure 2. Relaxation of V : $0 \rightarrow V_d$ (10^5 m/s) as $1/\nu$.

Cathode Fall Analogue: $v_i \rightarrow 3/\text{ns}$

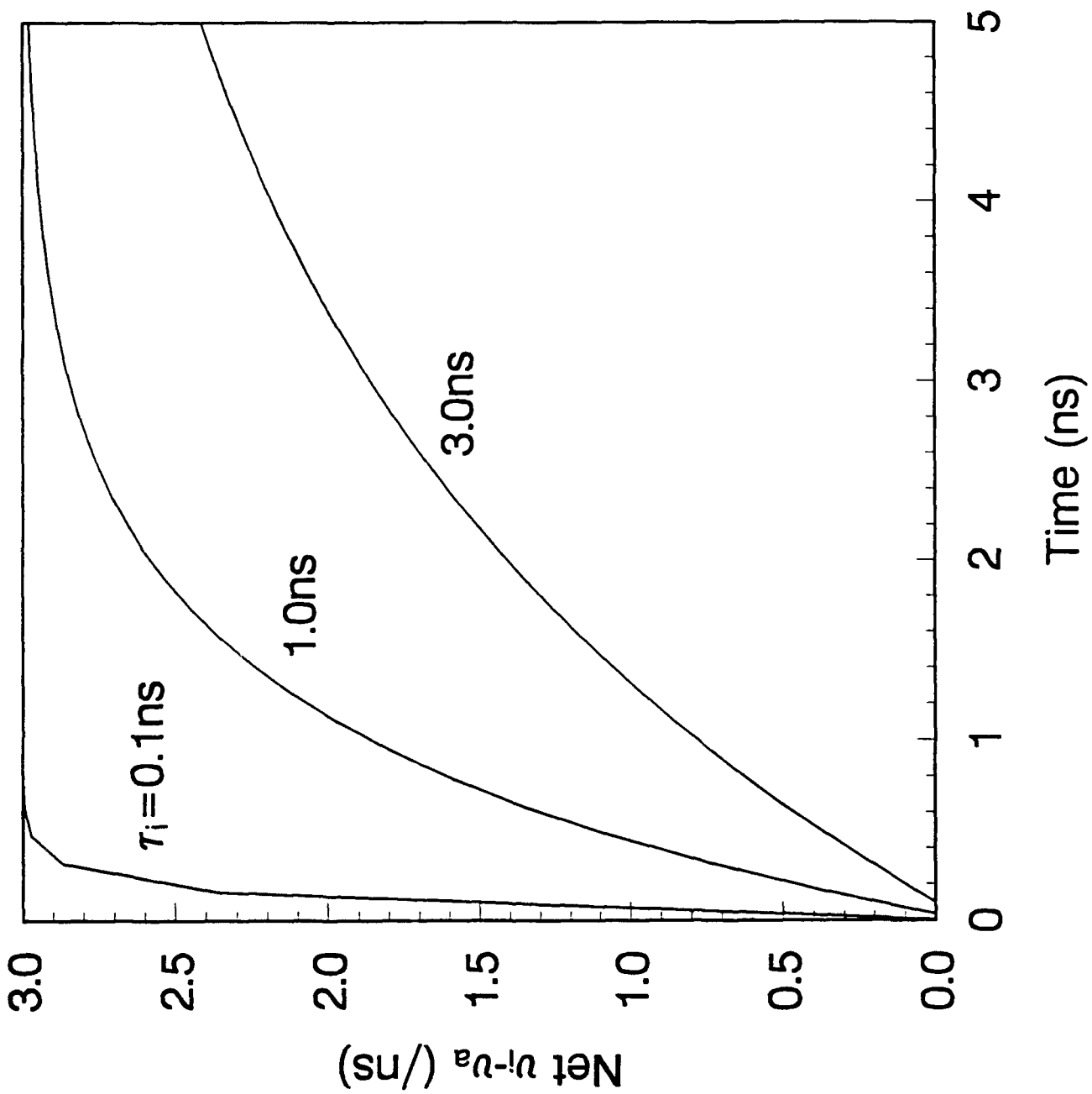
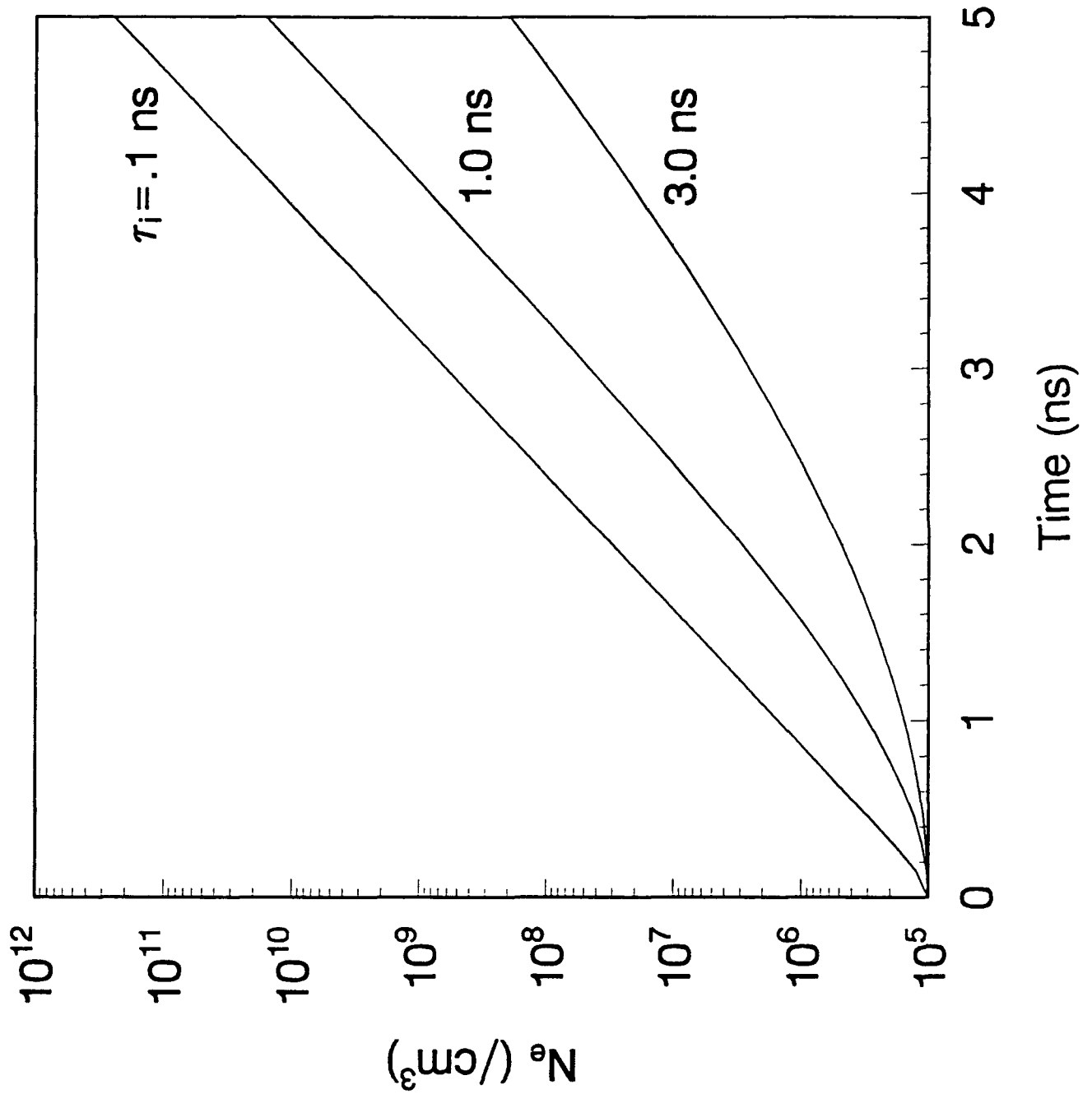


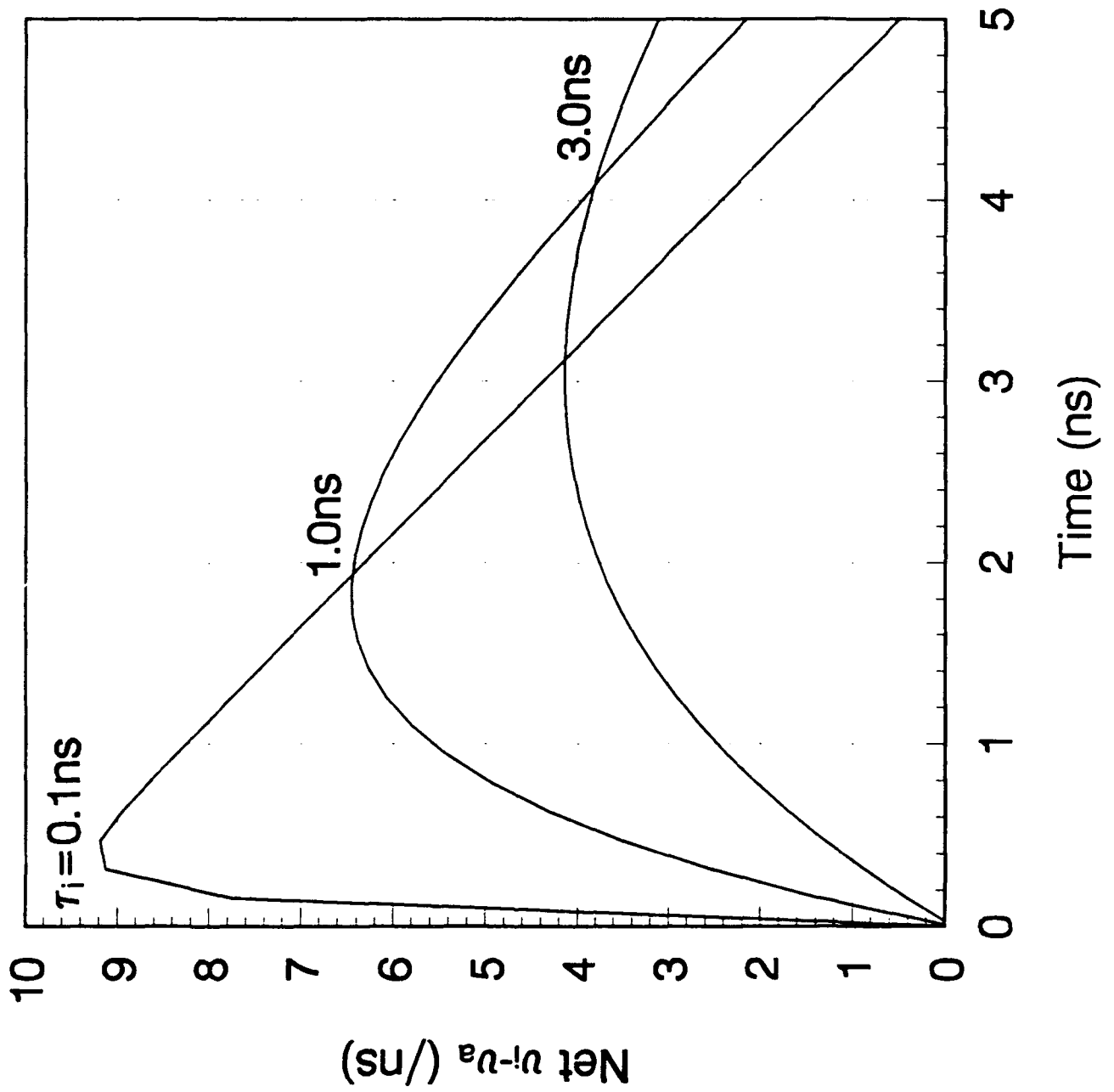
Figure 3. Net Gain-Loss Rates for Constant-E Case.

Figure 4. Electron Multiplication for Constant-E Case.

Cathode Fall Analogue: $v_i \rightarrow 3/\text{ns}$



Cathode Fall Analogue: $v_j \rightarrow 10. - 0.3 / \text{ns}$



Cathode Fall Analogue: $v_i \rightarrow 10. - 0.3 / \text{ns}$

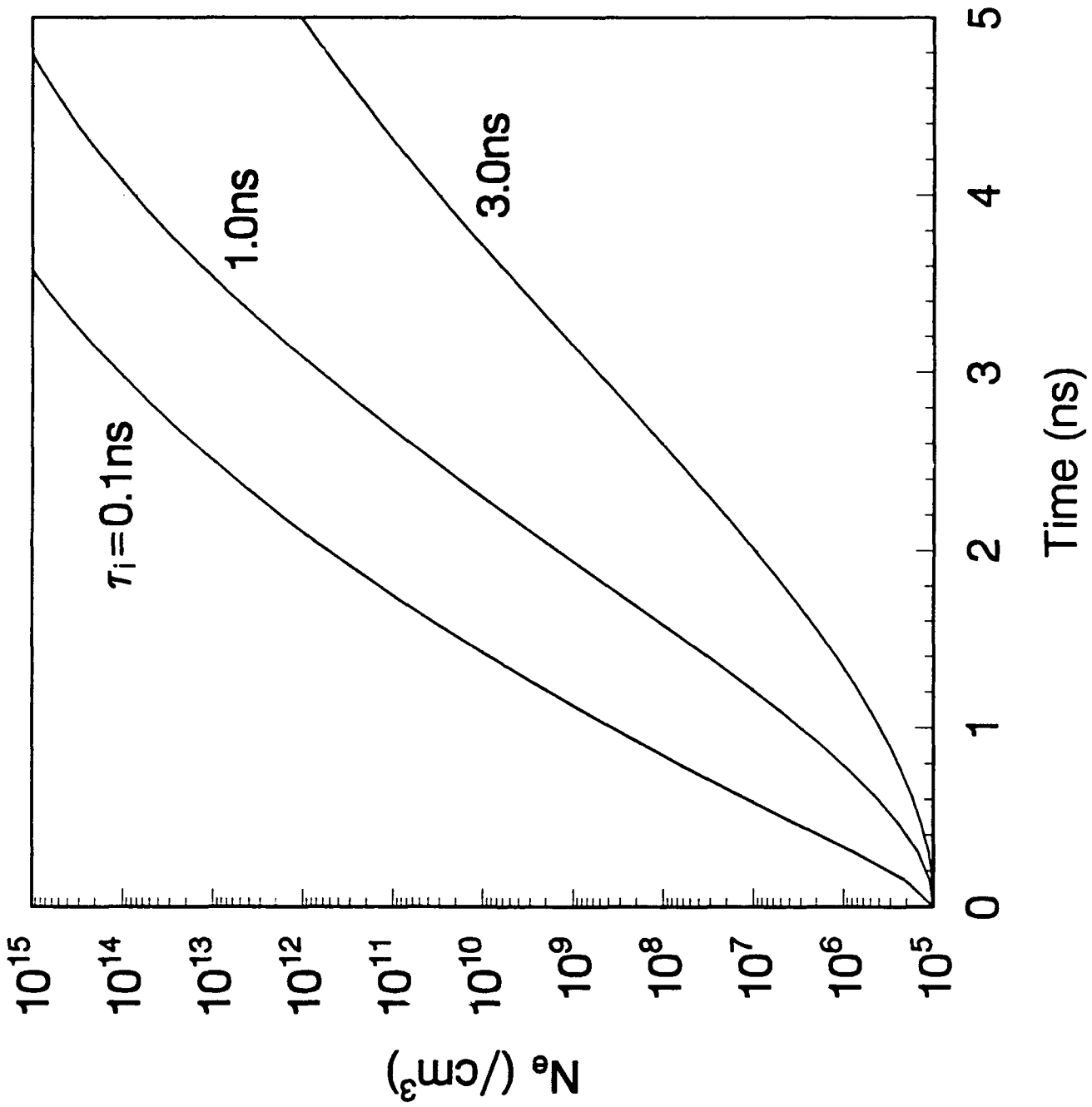


Figure 6. Electron Multiplication for Decreasing-E Case.

III. TIME-DEPENDENT BOLTZMANN ANALYSIS OF KINETIC RELAXATION.

The basis of the Quasi-Equilibrium Methodology being developed by Tetra is a quantitative characterization of the relaxation of the electron transport and kinetic coefficients for fast changes in local electric field, E . Such fast-changing E -fields are expected in avalanche-driven ionization waves, whether filamentary streamers or planar micro-gap breakdown discharges. This chapter documents the calculation of characteristic relaxation times for 1-atm dry air from solutions of the time-dependent Boltzmann equation.

The integro-differential Boltzmann equation is:

$$\left[\frac{\partial}{\partial t} + \nabla_r + \frac{e}{m} \mathbf{E} \cdot \nabla_v \right] f(\vec{r}, \vec{v}, t) = \left[\frac{\partial f}{\partial t} \right]_c$$

The operators in the first parentheses are the time derivative, the gradient in real space, and the inner product of the acceleration vector with the gradient in velocity space, respectively. The operand, f , is the electron distribution function, and the right-hand-side is the total effect of collisions. The balance between all heating and cooling mechanisms establishes the equilibrium distribution function. In the absence of quantized energy-selective processes, the steady-state solution is a Maxwellian distribution, proportional to $\exp(-\mathcal{E}/kT_e)$. However, energy-selective collisions distort the distribution function from a Maxwellian.

If the E -field varies on a larger scale-size than the distribution function, then the Local Field Approximation (LFA) applies, and the ∇_r operator may be neglected. We shall assume LFA applies either directly or through the use of the method of characteristics, which by following electron fluid particles (at the mean directed velocity), turns spatial variations into temporal variations. Any coefficient K_p may be calculated by convoluting the instantaneous f with the cross section σ_p for that process for which the cross section is σ_p as follows:

$$K_p = \frac{\int \sigma_p f \sqrt{2\mathcal{E}/m} d\mathcal{E}}{\int f d\mathcal{E}}$$

If the time scale on which the E -field varies is slow enough, then the steady-

state EEDF may be used to calculate equilibrium transport and kinetic rate coefficients.

The moments of the Boltzmann equation take the form of energy and momentum conservation and particle continuity equations. These can be solved using the equilibrium transport and kinetic rate coefficients, together with the coupled E-field equations to form a fluid model of a gas discharge. The Quasi-Equilibrium Methodology extends the fluid approach into the non-equilibrium domain by approximating the relaxation of the transport and kinetic coefficients by use of characteristic relaxation times. The purpose of our time-dependent Boltzmann analysis is to quantify the relaxation times for limited deviations from the equilibrium conditions.

For the analysis, we use the time-dependent Boltzmann equation solving code ELENDIF [Ref. 8], which uses implicit time integration techniques to insure stable relaxation to the steady-state solution. The electron-impact cross section data are from [Ref. 9] for N_2 , [Ref. 10] for O_2 , [Ref. 11] for Ar, and [Ref. 12] for H_2O . The time-dependent relaxation calculation includes superelastic collisions, attachment, recombination and ionization. We modified the code to use a geometric time progression, and to calculate an output at each time step: the non-equilibrium electron energy distribution function (EEDF), the transport coefficients, the energy flow rates, and the inelastic and superelastic rate coefficients.

The relaxation times can best be calculated for a step-function, instantaneous change in E-field, with initial conditions not too far from the new equilibrium. Therefore, we stepped up in E/N in increments of factors of 2 or so. The EEDF was initialized to a 0.1-eV Maxwellian, and the E/N was first set to 20 Td ($20 \times 10^{-17} \text{ V} \cdot \text{cm}^2$). Convergence was achieved in less than 1 ns, but the time-sequence continued for several ns. The E/N was then stepped up to 50 Td, using the 20-Td steady-state solution as the initial EEDF for the second geometric time sequence (0.1 ps to 4.6 ns). This continued up the E/N sequence 20, 50, 100, 200, 500 Td, and then we stepped down 200, 100, 50 and 20 Td. The resulting time-dependent EEDF sequence for the up-stepping half is shown in Figure 7.

The structure between 6 and 8 eV at very early times is due to superelastic

collisions with a nominal population of 10^{-4} $N_2(A)$ (i.e., one molecule in 10,000 is assumed in the $A^3\Sigma$ excited state). Other runs with 10^{-3} and 10^{-5} $N_2(A)$ showed the peak is indeed sensitive to the assumed excitation level, affecting the rate coefficients, especially for processes with thresholds in that vicinity, such as O_2 ionization. However, the relaxation behavior (discussed in detail below) is virtually unaffected. Nonetheless, it would be wise for a complete breakdown model to account for the dependence of rate coefficients on the $N_2(A)$ population.

We expected the high-energy tail to relax to a steady state on a slower time scale than the low-energy portion. It seems the normalization of the EEDF causes changes at all energies at all times. This agrees qualitatively with E. E. Kunhardt's results [Ref. 13] in pure N_2 . He solved the time-dependent Boltzmann equation with a totally different code, and observed that the EEDFs for different initial conditions relaxed to a common EEDF on the energy relaxation time scale, and then to the final steady-state on a slower scale.

A common approach to modeling non-equilibrium transport is that used by P. Bayle, J. Vaquie and M. Bayle [Ref. 14], which we shall call the BVB model. They assume all transport and rate coefficients are functions of electron temperature or mean energy $\langle \epsilon \rangle$. By solving the energy conservation equation, they calculate the non-equilibrium mean energy, and estimate the rate coefficients by interpolation as functions of that mean energy. That is reasonable if each non-equilibrium EEDF approximates an equilibrium shape at an intermediate E/N value. If that hypothesis is true, then the non-equilibrium coefficients we calculate by the time-dependent Boltzmann analysis should be smooth functions of $\langle \epsilon \rangle$. That suggests a simple graphical test of the hypothesis.

Figure 8 shows the time-dependent behavior of mean energy in our Boltzmann simulation. Since it is monotonic in each half (up and down in E/N), we can substitute $\langle \epsilon \rangle$ for time as the independent parameter. Figure 9 shows reduced collision frequencies ν/N vs $\langle \epsilon \rangle$. Notice that energy transfer is consistently over one order of magnitude slower than momentum transfer. It stands to reason that energy transfer, which depends on inelastic collisions, should be slower than momentum transfer, which is dominated by the more frequent elastic collisions. The lack of large deviations is encouraging. It explains why the BVB model gives reasonable behavior; the difference between a non-equilibrium collision

frequency and an interpolation between equilibrium values is never large. However, the systematic trend of the error, more obvious in energy transfer than in momentum transfer, is disturbing. The "orbits" reminiscent of hysteresis loops appear consistently in plots of all rate coefficients vs $\langle \mathcal{E} \rangle$, even the high energy-threshold rates shown in Figure 10. Close examination shows the rate coefficients are clearly relaxing faster than $\langle \mathcal{E} \rangle$. Thus, the slow relaxation of $\langle \mathcal{E} \rangle$ (not to be confused with the relaxation of the energy transfer rate) casts doubt on the basic premise of the BVB approach.

A closer examination of details of the Boltzmann output (specifically the energy balance) revealed an explanation. The instantaneous net energy rate can be expressed as follows:

$$\langle \dot{\mathcal{E}} \rangle = \frac{e}{m} E V_e - \langle \mathcal{E} \rangle \nu_{\mathcal{E}}$$

The heating term $E V_e e/m$ is changing on the same time scale as the energy transfer collisional frequency $\nu_{\mathcal{E}}$. Consequently, the two nearly balance, so the mean energy $\langle \mathcal{E} \rangle$ changes much more slowly than $1/\nu_{\mathcal{E}}$.

We propose an alternate methodology based on quantifying a characteristic relaxation time. Figure 11 shows how the time-dependent elastic collision frequencies relax toward equilibrium. Most of them show close to an exponential decay of the difference $|K-K_q|$ (a straight line on a log-linear plot). The desired relaxation times, τ , must be extracted from the temporal behavior of the calculated coefficients, K . Assuming the governing equation is of the form

$$\dot{K} = (K_q - K)/\tau$$

where K_q is the equilibrium value, the average relaxation time in a finite time step Δt can be estimated as

$$\tau = \Delta t / \ln \left[\frac{K_q - K}{K_q - K'} \right]$$

The results of that calculation for momentum transfer, which we expected to relax on a time scale comparable to energy transfer, and for ionization, which we

expected to relax on much slower time scales, is shown in Figure 12.

The algorithm used is clearly inaccurate at late times when $|K_q - K| \ll K_q$, and differencing errors make the results meaningless. Calculations at those times are not included in Figure 12. Nonetheless, the behavior of the calculated τ values is rather peculiar. The calculations at very early times are not particularly meaningful, either. The algorithm is most accurate when $\Delta t \approx \tau$. The " $\tau = t$ slant lines" in Figure 12 are near that optimal point. If we use the intersecting points (within the box for each E/N value) as "nominal" τ values, we find that the high-energy processes are barely slower to relax than momentum transfer, and both are about 10 ps, which is just about what we expected for the energy transfer relaxation time, as shown in Chapter II.

Notice that the ionization τ -curves consistently approach the nominal intersection point from above, and the momentum transfer τ -curves consistently approach it from below. This consistent pattern indicates a physically significant difference in the relaxation behaviors. However, it is not clear how to exploit this observation.

There are two main conclusions: 1) The momentum transfer collision frequency relaxes on about the energy transfer time scale (~10 ps). 2) The high energy-threshold rates relax on too fast a time scale (compared to the rates themselves) for non-equilibrium effects to be of much consequence. Therefore, the Quasi-Equilibrium Methodology can be based on the assumption that each coefficient K relaxes to its equilibrium value K_q as:

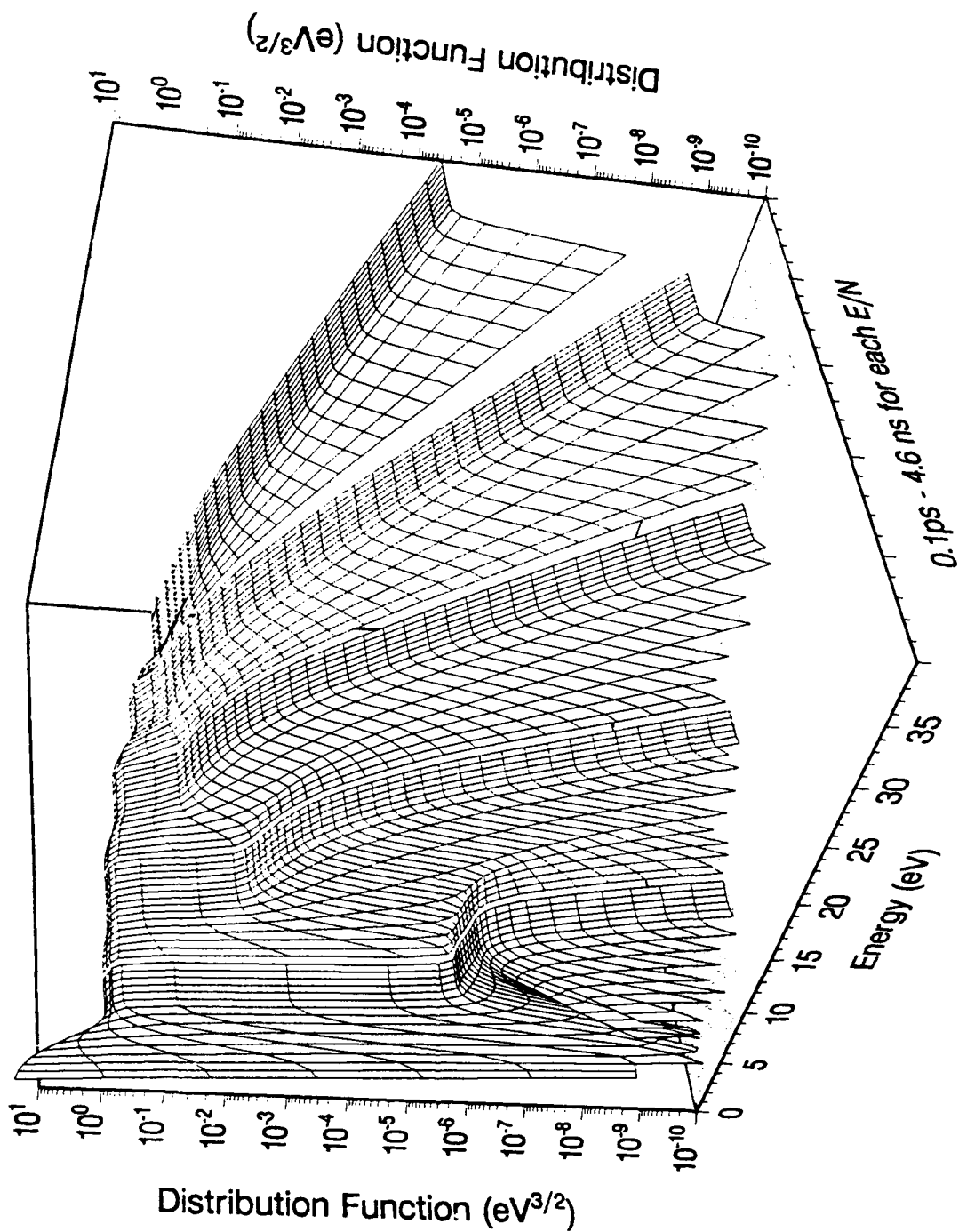
$$\dot{K} = (K_q - K)/\tau$$

If a detailed Boltzmann analysis is unavailable, one may use, to first order, the energy relaxation time:

$$\tau \approx \frac{1}{\nu_g} = \frac{\langle \mathcal{E} \rangle}{eEV_d}$$

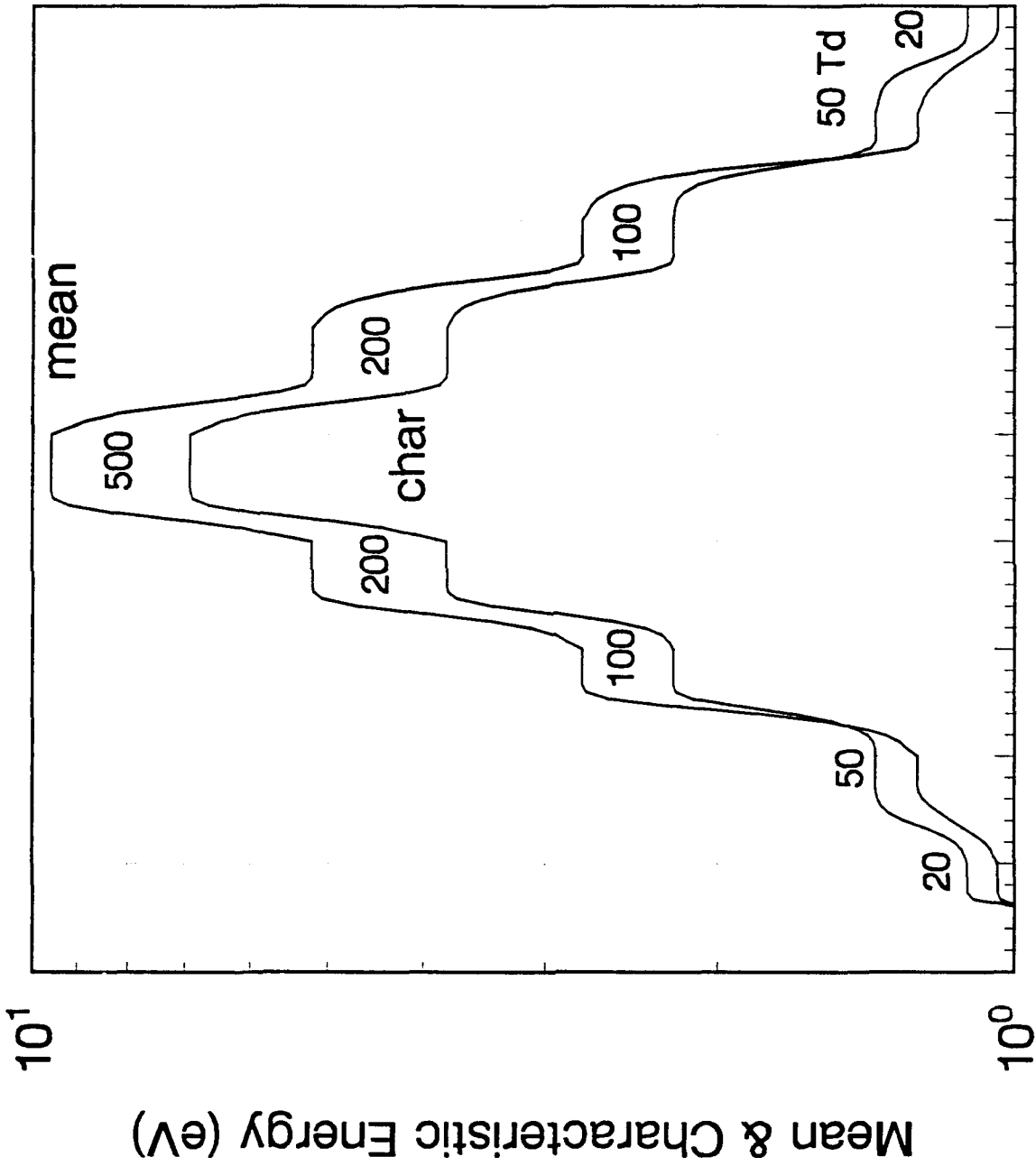
Consecutive Relaxations in Dry Air

Figure 7. Sequence of Time-Dependent EEDFs.



Successive Relaxations Up & Down E/N

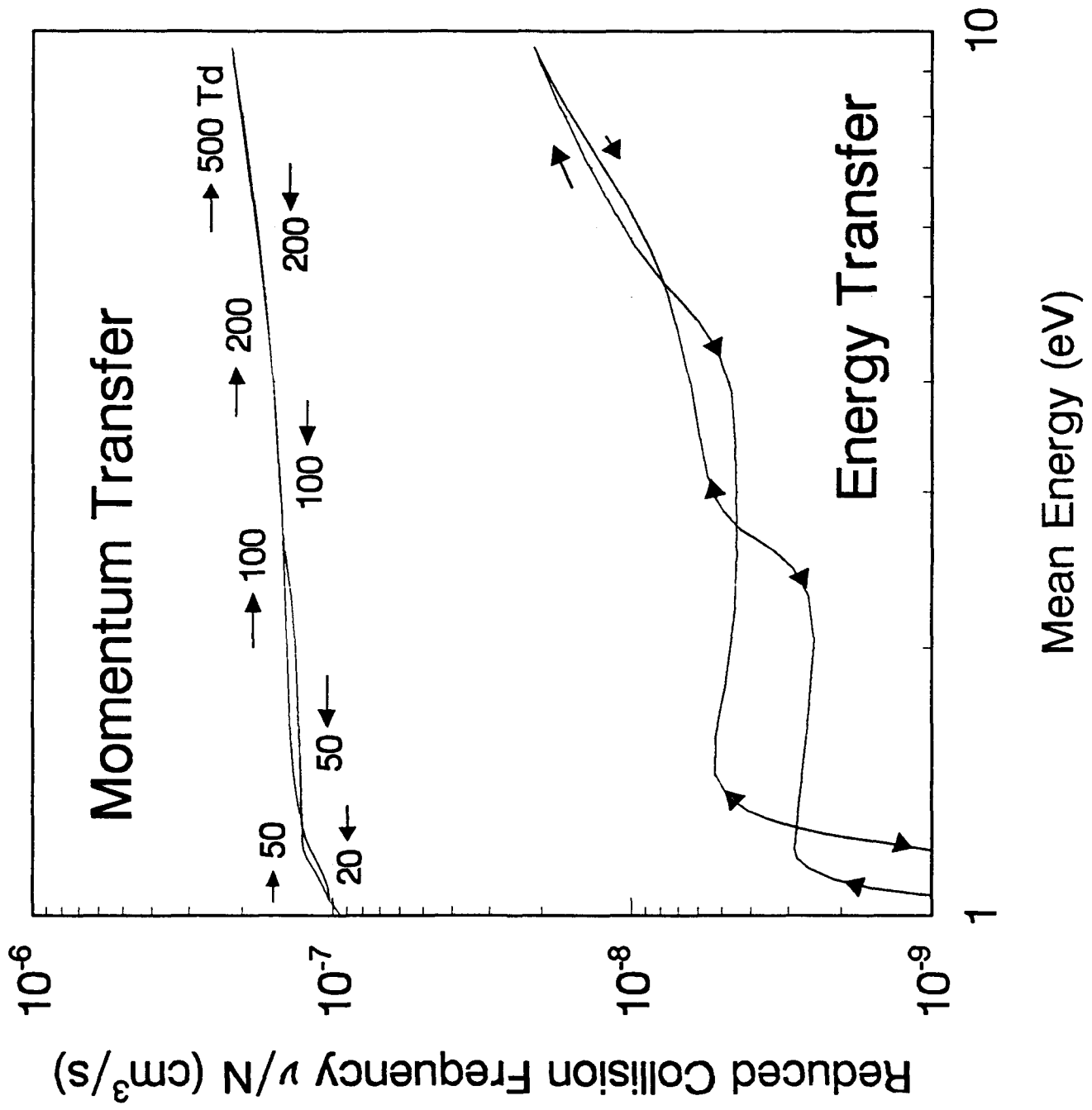
Figure 8. Non-Eq. Mean Energy for Successive Relaxations.



0.1ps - 4.6ns for each E/N

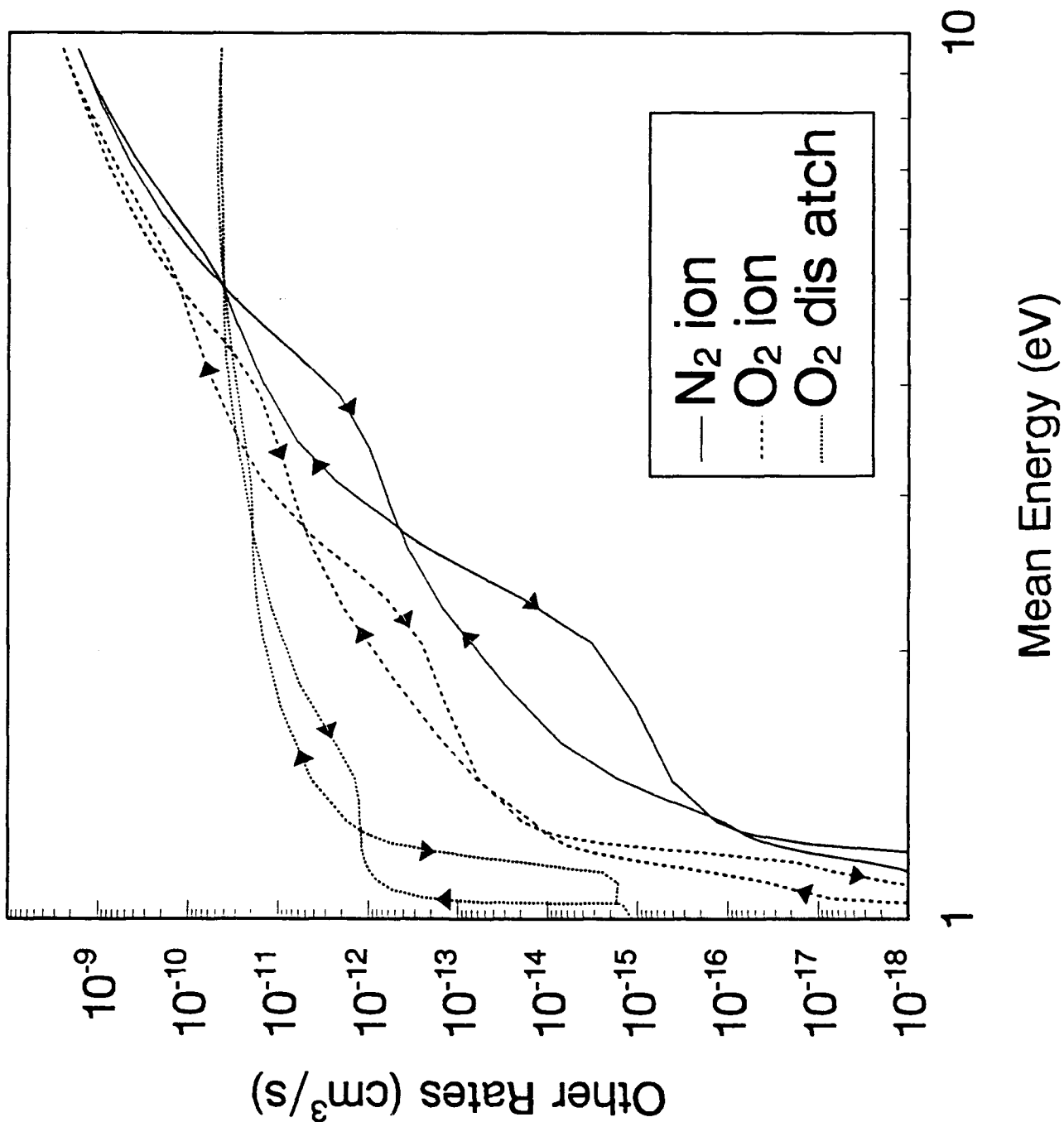
Successive Relaxations Up & Down E/N

Figure 9. Collision Frequency Orbits in Energy Space.



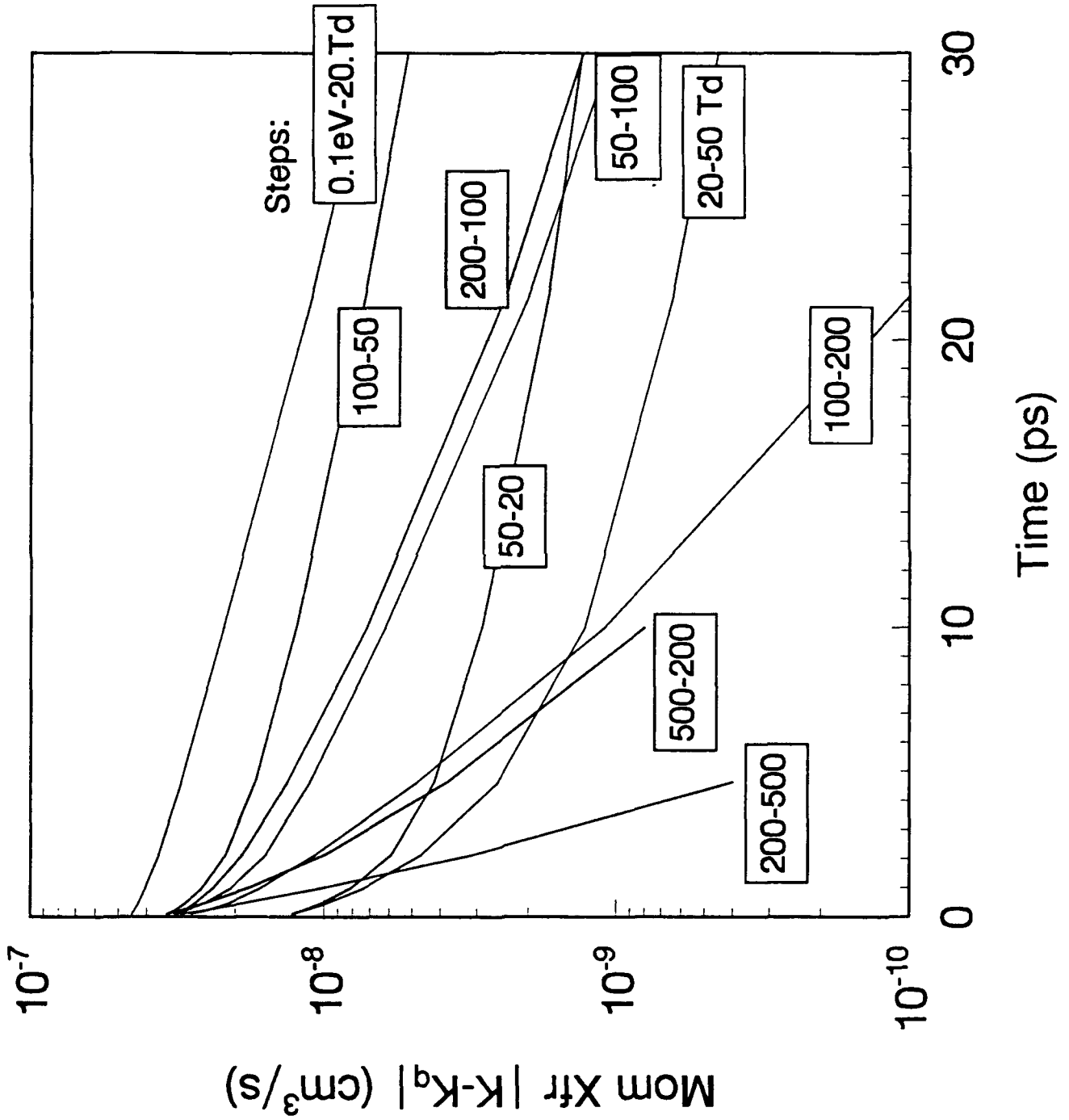
Successive Relaxations Up & Down E/N

Figure 10. Selected Kinetic Rates Orbits in Energy Space.



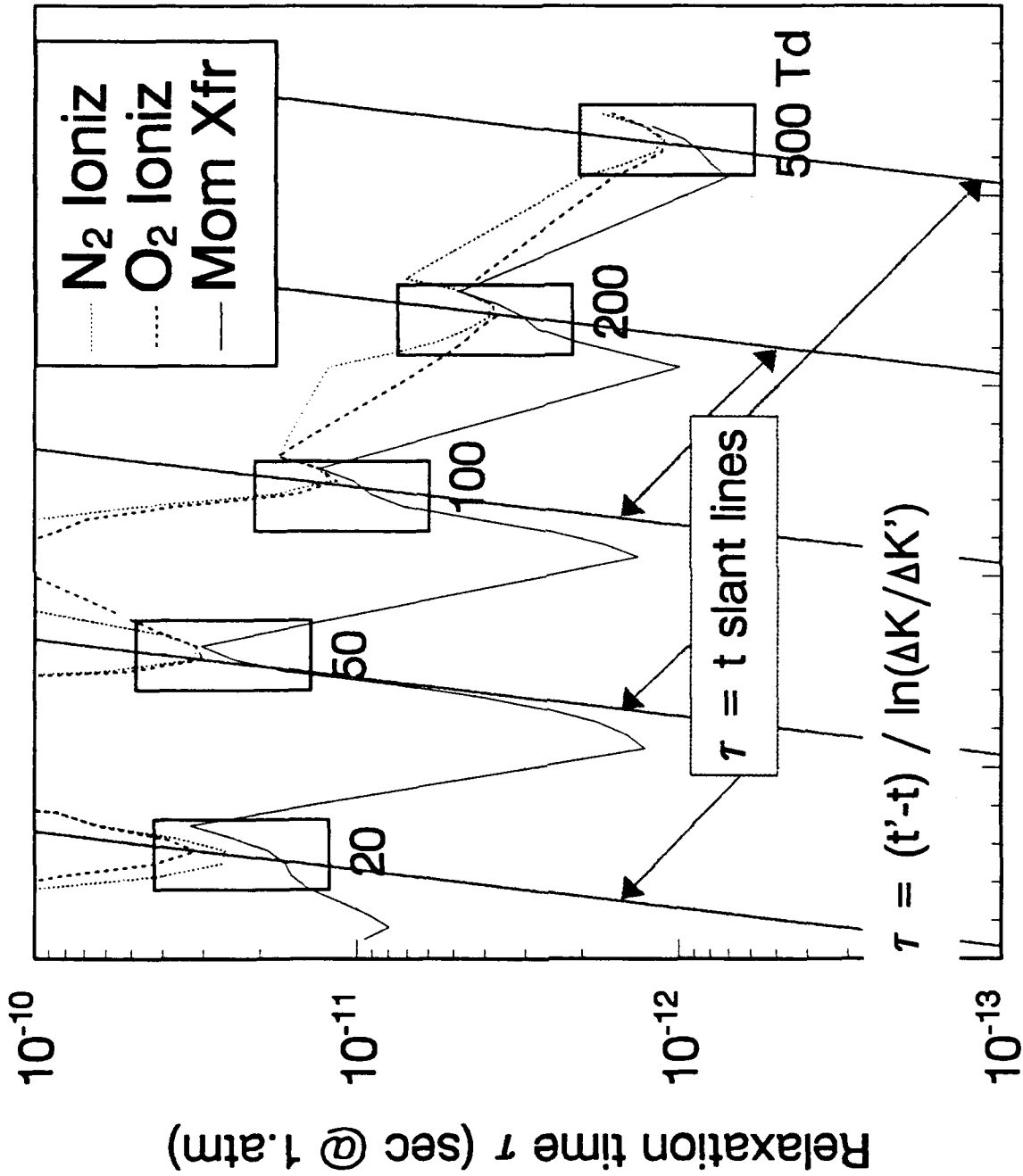
Successive Relaxations Up & Down

Figure 11. Elastic Collision Relaxations in Time.



Consecutive Relaxations in Dry Air

Figure 12. Calculated Relaxation Times.



Time = 0.1 ps to 4.6 ns for each E/N

IV. NON-EQUILIBRIUM EFFECTS ON STREAMER PROPAGATION.

The Quasi-Equilibrium Methodology (QEM) purports to model non-equilibrium effects in fast ionization waves. A cogent argument was made in Chapter II that non-equilibrium effects, especially the velocity overshoot effect, would have a profound effect on streamer propagation. The purpose of this chapter is to document a numerical test of this hypothesis in the 1-dimensional electric field solver ELF1D.

The ELF1D code solves the current continuity equation

$$\nabla \cdot (J + \dot{D}) = 0$$

where $J = eN_e V_e$ is conduction current, and $D = \epsilon E$ is the displacement vector, whose time derivative is displacement current. The ELF1D code includes a gas kinetics module which updates the conductor density eN_e and velocity V_e over a finite time-step Δt , given initial and final E-field arrays.

The code was made operational on an 80386-based PC using the Lahey Fortran compiler to produce protected-mode code, thus avoiding the memory limitations of DOS. The gas kinetics module was modified to use the QEM current integration algorithm, coded in subroutine CURINT. That routine integrates the two pairs of ordinary differential equations (ODE)

$$\begin{aligned} \dot{N}_e &= S - R N_e & \dot{R} &= (\beta_q - \alpha_q - R)/\tau \\ \dot{V}_e &= \frac{e}{m} E - \nu V_e & \dot{\nu} &= (\nu_q - \nu)/\tau \end{aligned}$$

where S is an external ionization source; the loss rate, R , tends to the net difference between equilibrium attachment (β_q), and Townsend ionization (α_q) rates; the collision frequency, ν , tends toward the equilibrium value, ν_q . The relaxation times, τ , for both ODE pairs were set to the energy transfer time:

$$\tau = \frac{\langle \epsilon \rangle}{e E V_d}$$

In order to determine the effect of the QEM corrections, it was necessary to artificially defeat them. For 1 atm air near 3 MV/m, the energy transfer time is about 10^{-11} s, but the momentum transfer frequency is about $5 \times 10^{12}/\text{s}$. Therefore, by artificially reducing the relaxation time by a factor of 10^{-3} , we made the relaxation of transport coefficients virtually instantaneous.

The test case chosen was a spherical ionization wave driven by a rising voltage. The spherical geometry simulates the region ahead of a filamentary streamer tip, and insures a field enhancement sufficient to launch an ionization wave. A similar simulation in SF_6 is reported by R. Morrow [Ref. 15] with the same essential qualitative features. While both cases are better described as voltage-driven growing coronas, they contain the essential phenomenological features of freely propagating streamers. In our case, the gap goes from 1 mm to 1 cm radii, insuring a vacuum field enhancement factor of 10; the driving voltage rises to 30 kV in 10 ns. External ionization is negligible, but the electron density is initialized to $10^{15}/\text{m}^3$ to simulate the photoionization ahead of the glowing streamer tip [Ref. 16].

The results are compared in Figures 13 and 14, each of which contains two "frames" from the time-dependent simulations with and without the QEM correction. The qualitative behaviors are very similar: the streamers are launched at about the same time, and propagate at about the same velocity. The electron avalanching starts when E exceeds 3 MV/m, and the exponentially growing electron density eventually shunts the electric field. After a few transient oscillations, the field will equilibrate at the critical value of 3 MV/m. In effect, the discrete grid cells are acting like glow discharge voltage regulators in series, attempting to clamp the E -field at 3 MV/m. In the limit of very slow voltage rise rate, the solution would be a series of steady-states with the E -field clamped to 3 MV/m in the corona, and falling off as $1/R^2$ outside the corona. That clamping requirement and the voltage rise rate determine the "streamer" velocity to first order.

The striking difference between the two simulations is in the values of electron density created by the ionization waves: about $10^{21}/\text{m}^3$ without QEM, but only $10^{19}/\text{m}^3$ with QEM. An explanation can be found in the electron velocity overshoot. Because the collision frequency takes many collisions to relax to

equilibrium, the instantaneous velocity overshoots the equilibrium drift velocity value V_d . This tendency of the electron fluid to initially over-react to the fast-rising E-field makes it create the charge-separation necessary to shunt the E-field more quickly. As a result, fewer electrons are just as effective in shunting the local over-voltage, and the transition occurs sooner, creating much lower ionization levels.

The lower electron density created by an ionization wave can prolong the breakdown time significantly. The breakdown time is roughly the time it takes ohmic heating to raise the temperature to about 10^4 K, and the ohmic heating rate is proportional to N_e . Although N_e does not remain constant after the streamer crosses the gap, the initial electron density created by the streamer does significantly affect the total breakdown time. Thus, the QEM approach to modeling the initial phases of air breakdown is essential.

Another less obvious difference is that the simulation without QEM got bogged down after about 3.1 ns, with the time step becoming comparable to a collision time (a few ps). But the simulation with QEM continued quite well beyond 6 ns, with time steps at worst comparable to the energy transfer time (0.1 ns). The later time behavior is displayed in Figures 15 and 16, which display, respectively, E and N_e curves at the frames nearest the chosen times. This ability of the QEM algorithms to take reasonably large time steps will be very valuable in Phase II.

Figure 13. Two frames from streamer simulation without QEM.

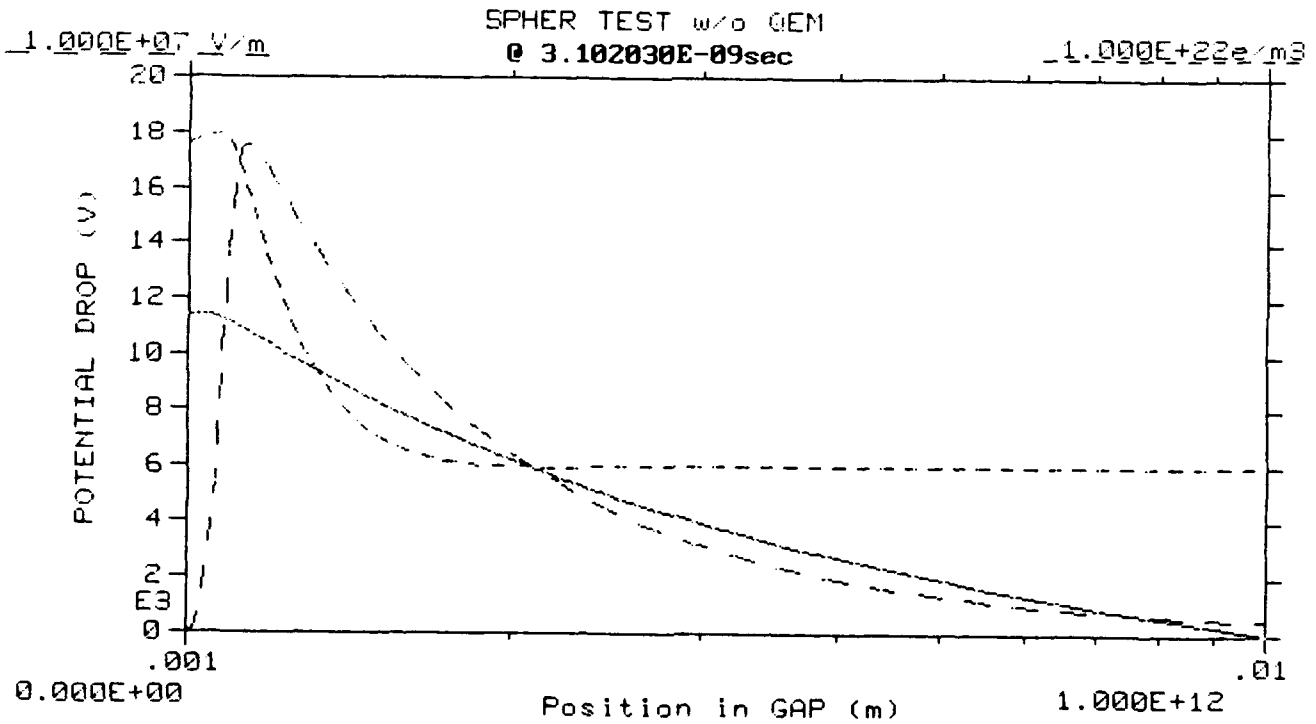
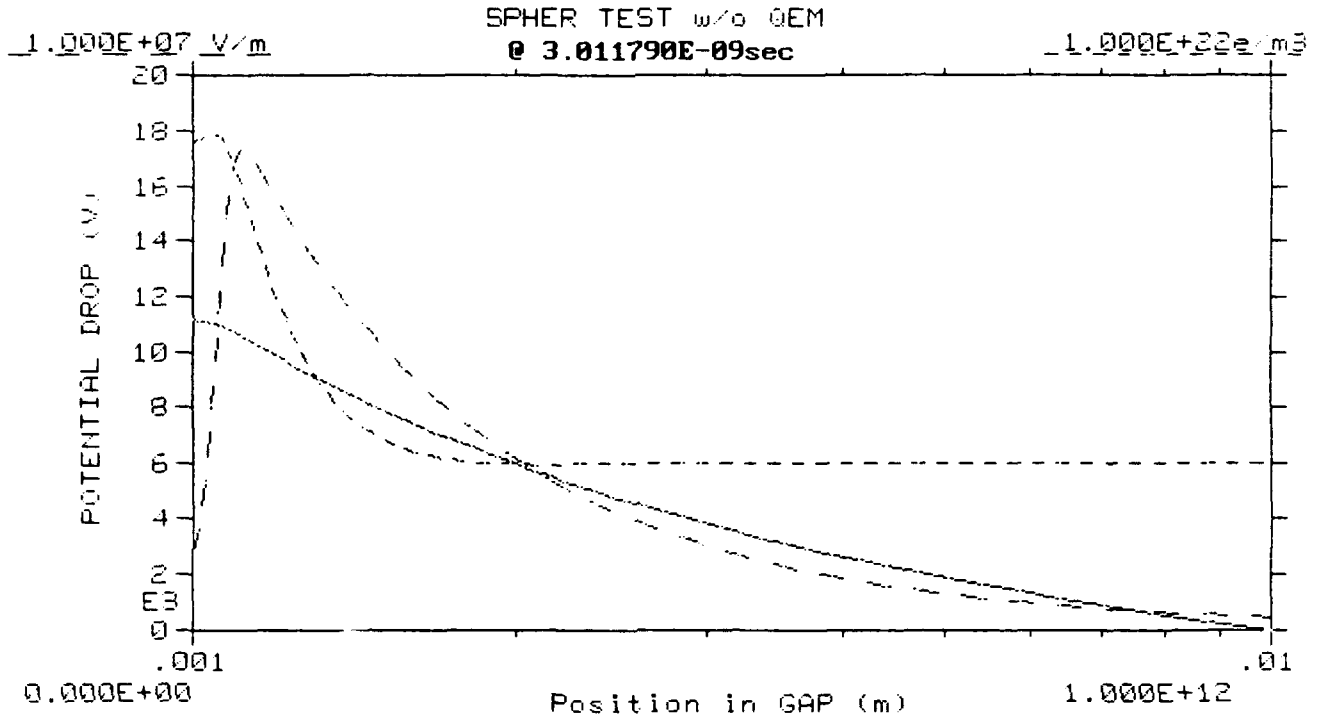


Figure 14. Two frames from streamer simulation with QEM.

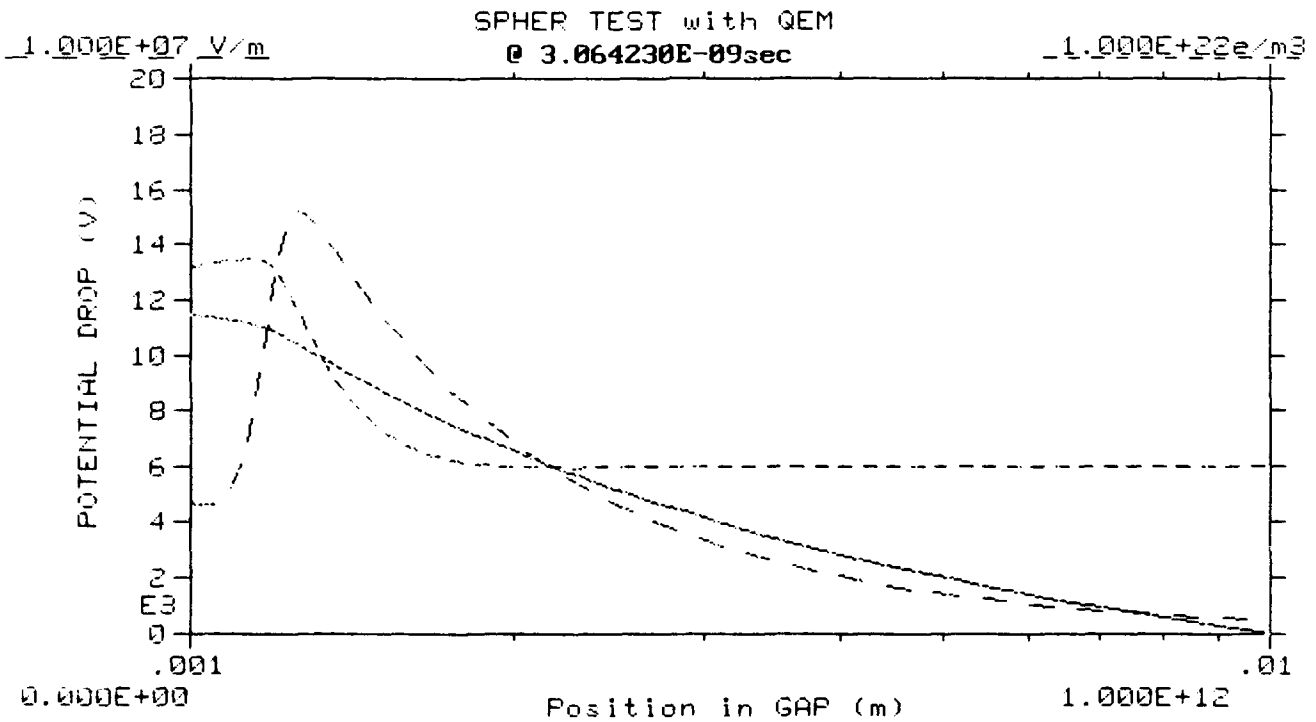
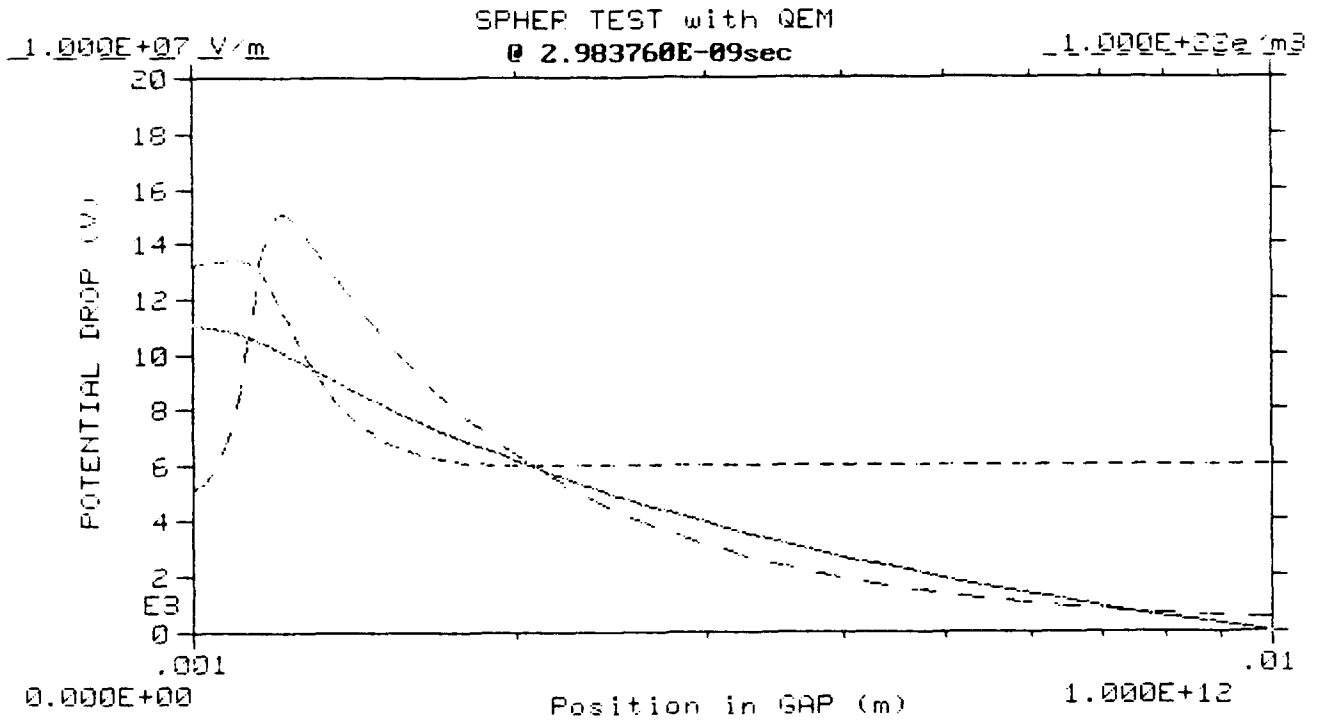


Figure 15. E-profiles for streamer simulation with QEM.

Spherical Test With QEM

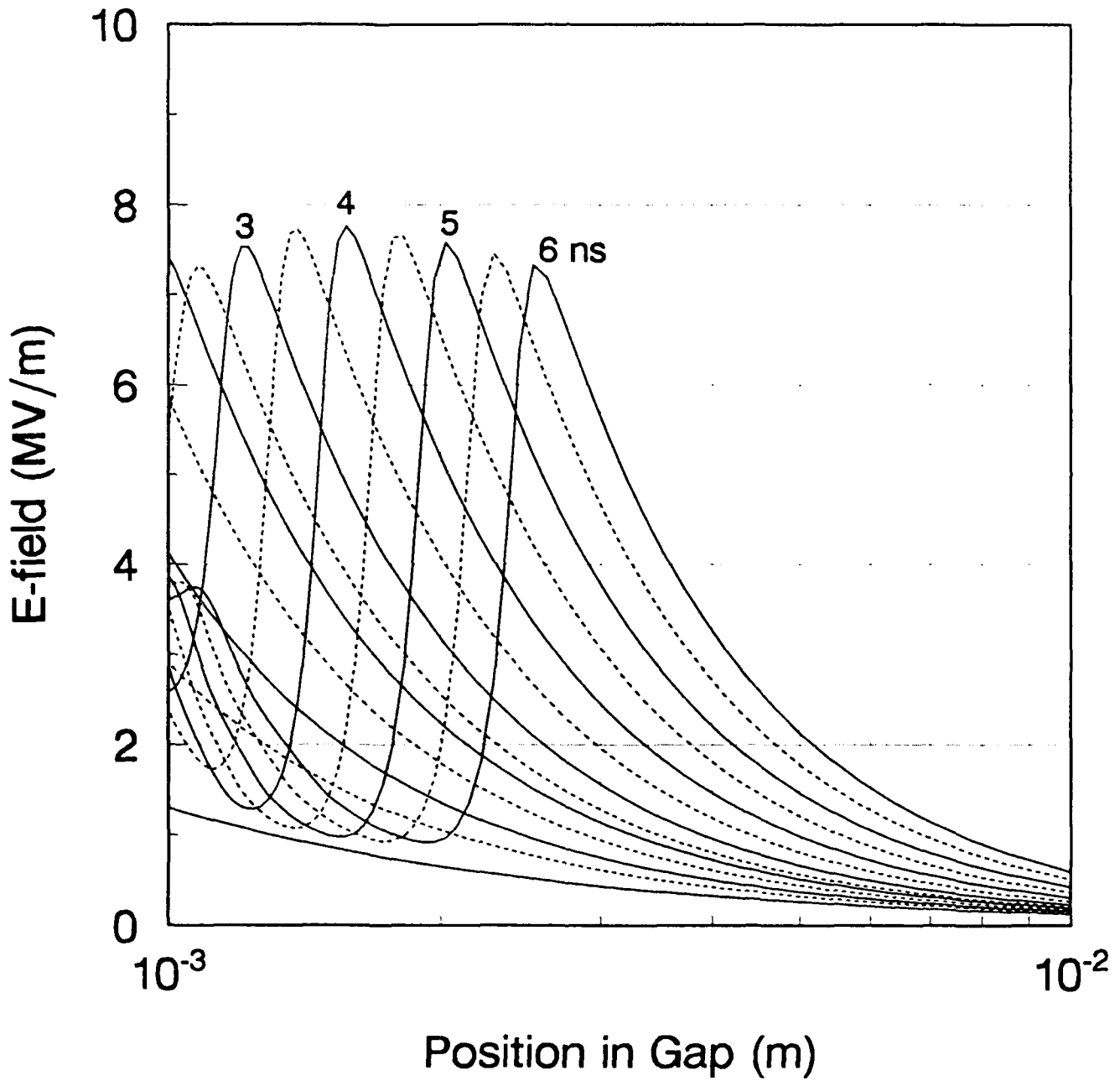
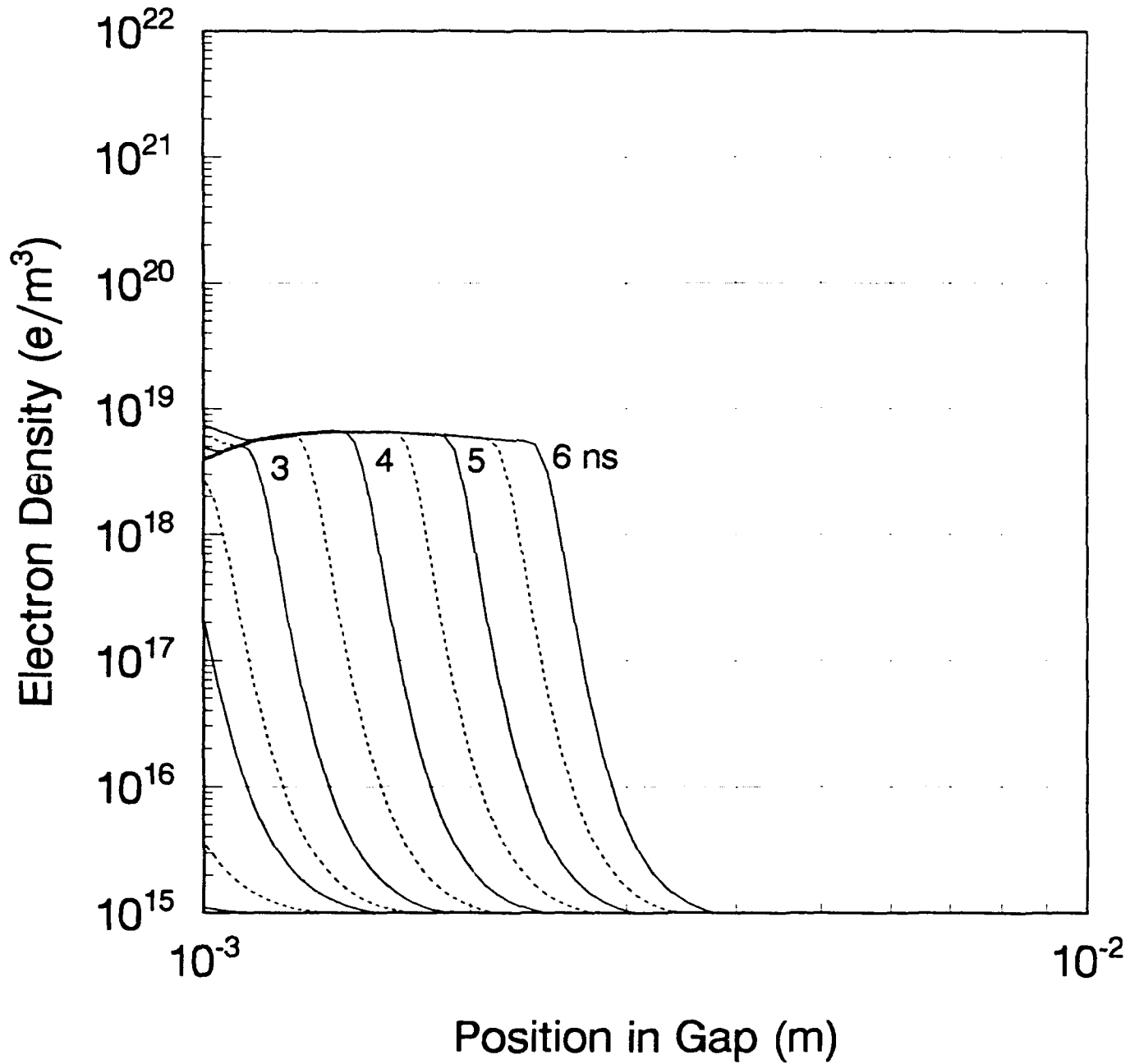


Figure 16. N_e -profiles for streamer simulation with QEM.

Spherical Test With QEM

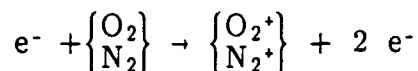


V. SIMPLIFICATION OF THE AIR BREAKDOWN KINETICS MODEL.

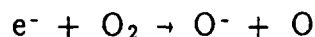
The air breakdown (BD) model developed by Tetra [Ref. 15] tracks the populations of 16 components with several dozen reactions among them. For a 0-dimensional model, computational cost is not significant, but for an N-dimensional code, the large number of nodes justifies simplification of the point-by-point kinetic computations. This chapter describes our effort to simplify the air BD kinetics model.

The kinetics of an electric discharge in air are rather complex, and an over-simplified model is doomed to a very narrow domain at best. Some mechanisms are obviously necessary in any air BD model, including both electron-impact phenomena and heavy-heavy collisions. We shall discuss them in approximate order of importance, with the actions we took to simplify the model, including validation test runs, leading to our recommendations for a simplified model.

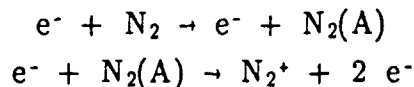
It is clear that any model of air BD must include the dominant sources and sinks of electrons. Those are, respectively, electron multiplication by molecular ionization:



and dissociative attachment:

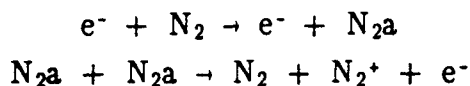


Electronic excitation followed by ionization of the excited species:



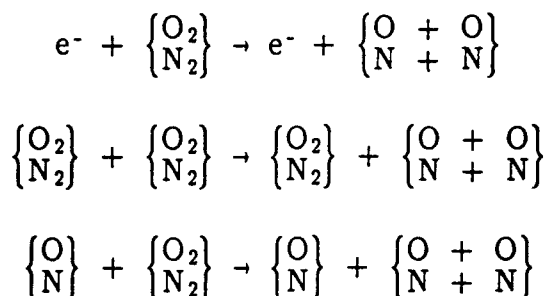
was found to be important. $N_2(A)$ stands for the $A^3\Sigma$ state at 6.17 eV. The many paths by which electron impacts populate $N_2(A)$ can be combined as shown in Figure 17 with no loss of phenomenology, and our benchmark calculations proved it to have no effect on the model behavior. A secondary mechanism is

excitation of the $a^1\Sigma$ state at 8.40 eV (denoted " N_{2a} ") followed by self-quenching ionization:

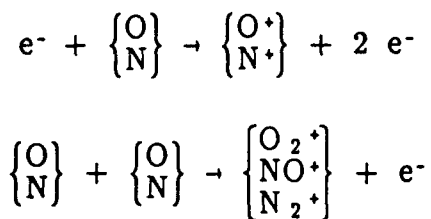


Elimination of that path increased the simulated closing time for the test case (25kV/cm) from 156 ns to 164 ns. The small gain in computational efficiency is not worth the loss in accuracy.

Because atomic O and N react to produce significant ionization, the dominant sources and sinks of atomic species must be included. The significant sources of dissociation are impact with electrons, molecules and atoms:

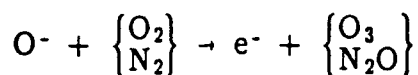


Electronically excited O_2 levels above the dissociation energy immediately dissociate. That mechanism dominates over direct dissociation of O_2 , as shown in Figure 18. Summing all paths into one effective dissociation rate had no discernible effect on model behavior. The atomic population then produces ionization by electron impact or by association:



The key to correct model behavior (why the gap closes at all) for an under-

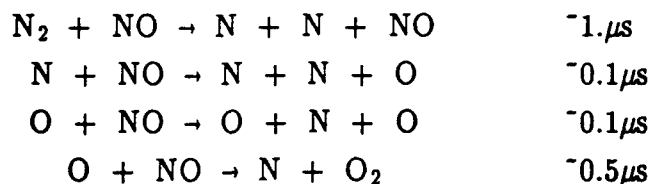
volted gap is molecular-impact associative detachment:



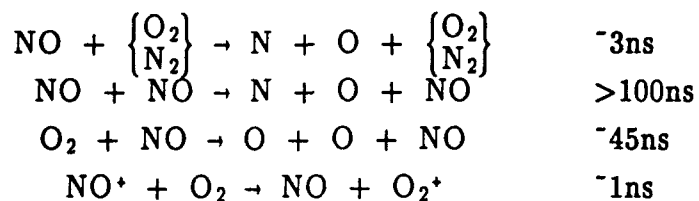
which is also the major source of the complex molecules O_3 and N_2O in air discharges.

The above processes are clearly necessary, but they are not sufficient. Other processes in the full model affect the BD behavior in subtle ways not as easily understood. Therefore, we sought to identify negligible processes so we could simplify the model by elimination, rather than building up from what we know is needed. A nominal characteristic life-time for the "first" component of each reaction can be computed based on the maximum population of the "second" component during the full model simulation. (The choice of "first" and "second" is a subjective judgment.) The density traces for the 25 kV/cm test case are shown in Figure 10.

Based on that methodology, we determined that quenching of the $N_2(A)$ by N or NO is negligible compared to self-quenching. We found many NO-impact reactions could be eliminated with no ill effect. The other eliminated reactions are:

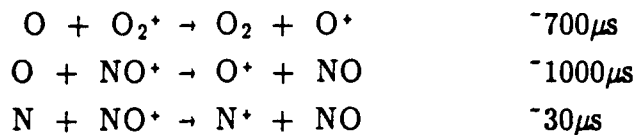


but we kept the following reactions:

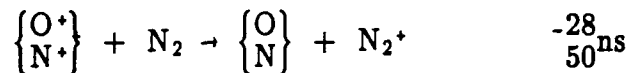


The last is actually a charge-exchange process. Other charge-exchanges were

neglected because of their slow nominal characteristic times even at 10,000 K, as shown:



But we kept the following faster charge-exchanges:



and the "atom-exchange" reaction



With the above eliminations only, the BD model behavior is unaffected for the test case. Some other reactions may also be negligible, but the gains are diminishing for the work required to validate the model after each elimination. As it stands, the simplified air BD model is fast enough to run interactively in 1-2 minutes on a VAX 11-780.

The computational cost is more sensitive to number of components (there is one ODE per component) than to number of reactions (each reaction merely contributes a loss or gain term in a summation). Therefore, we need ways to reduce components entirely. The most promising strategy is to neglect chemical composition. That would reduce the number of species (and number of ODEs) from 16 to the following 9:

$$e^-, M_2 = \begin{Bmatrix} \text{N}_2 \\ \text{O}_2 \\ \text{NO} \end{Bmatrix}, M_2^+, A = \begin{Bmatrix} \text{N} \\ \text{O} \end{Bmatrix}, A^+, O^-, N_2(A), N_2a, M_3 = \begin{Bmatrix} \text{O}_3 \\ \text{N}_2\text{O} \end{Bmatrix}$$

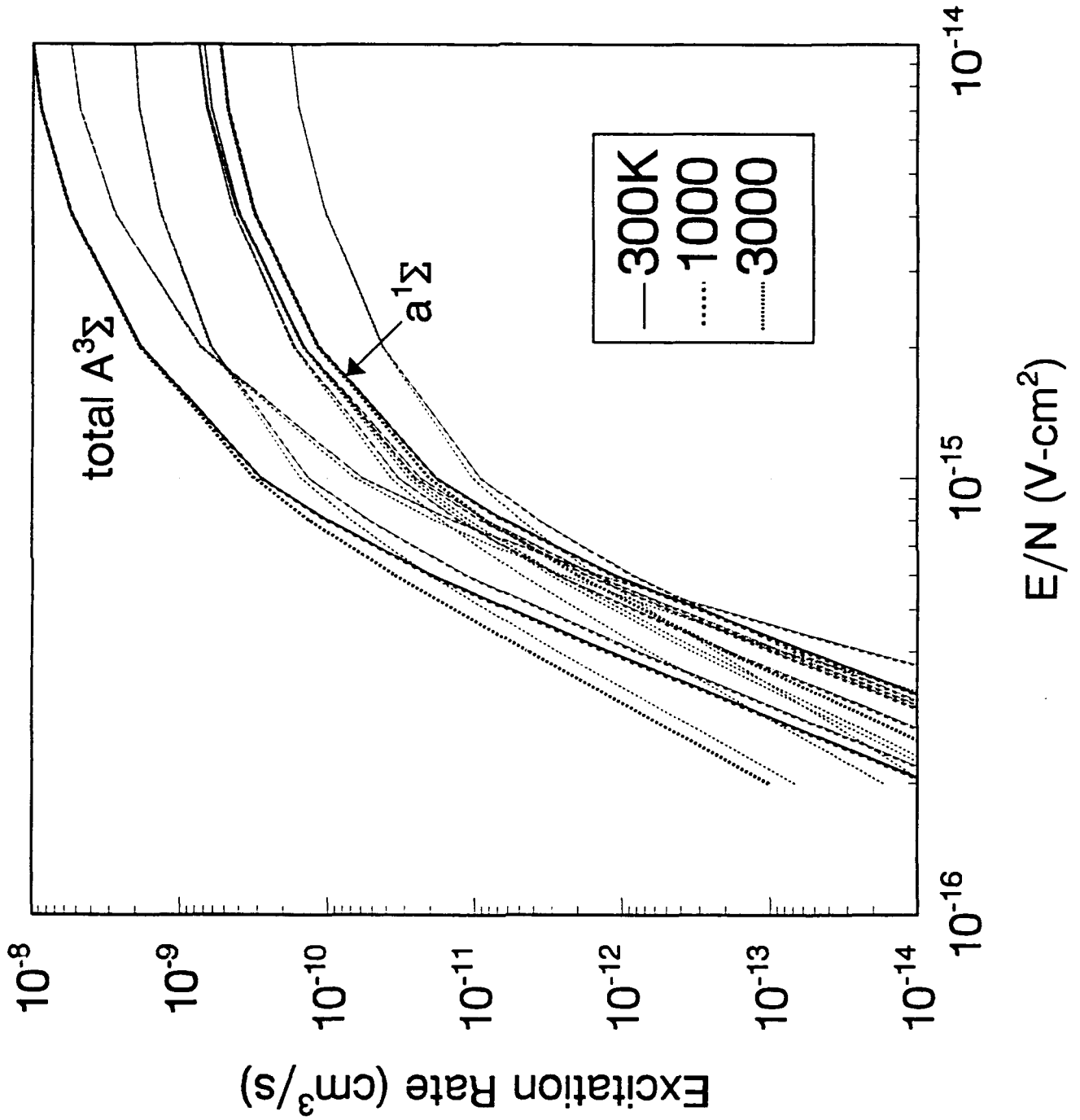
The NO reactions can be included in a weighted average if we can calculate a nominal NO fraction. Since the NO fraction is significant only near the end of the test case simulation, we suggest treating it as a function of temperature. Thus, the simplified model should reproduce the test case used for calibration

exactly. However, the range of applicability of the simplified model for different conditions needs to be determined with other test cases. That complicates the validation procedure.

The cost in manpower must be carefully assessed against the gains in computational speed. The above method should produce about a factor of 2 speed-up, but the validation procedure requires a calibration test case "typical" of the application, and sufficient exploration of the multidimensional variable space to determine the domain of applicability. That is beyond the Phase I scope, but may be fruitful in Phase II.

N₂ Electronic Excitation

Figure 17. Dominant N₂ Excitation Rates.



O₂ Electron-Impact Dissociation

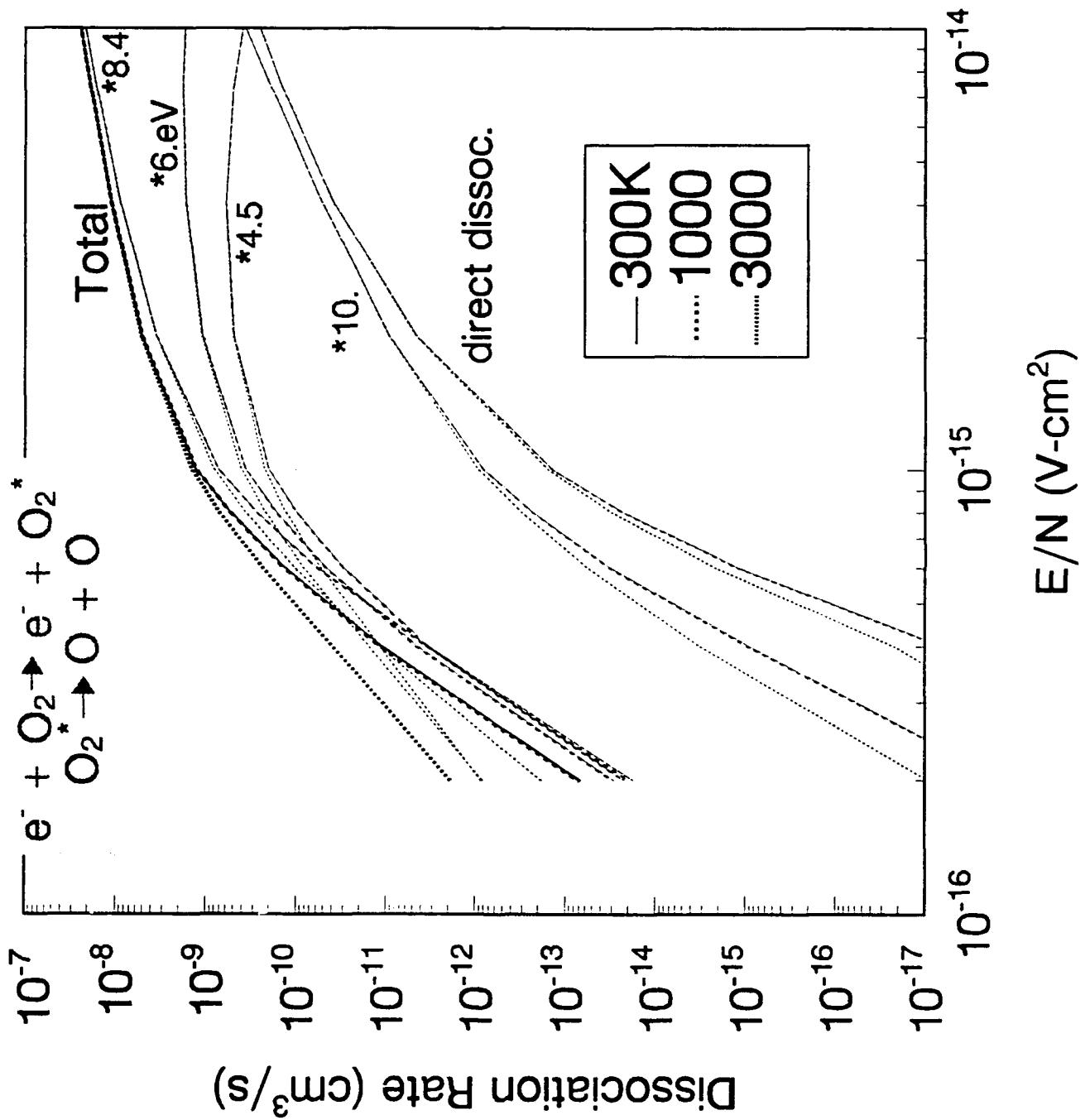


Figure 18. Dominant O₂ Dissociation Rates.

Air Spark Glow Phase (25 kV/cm)

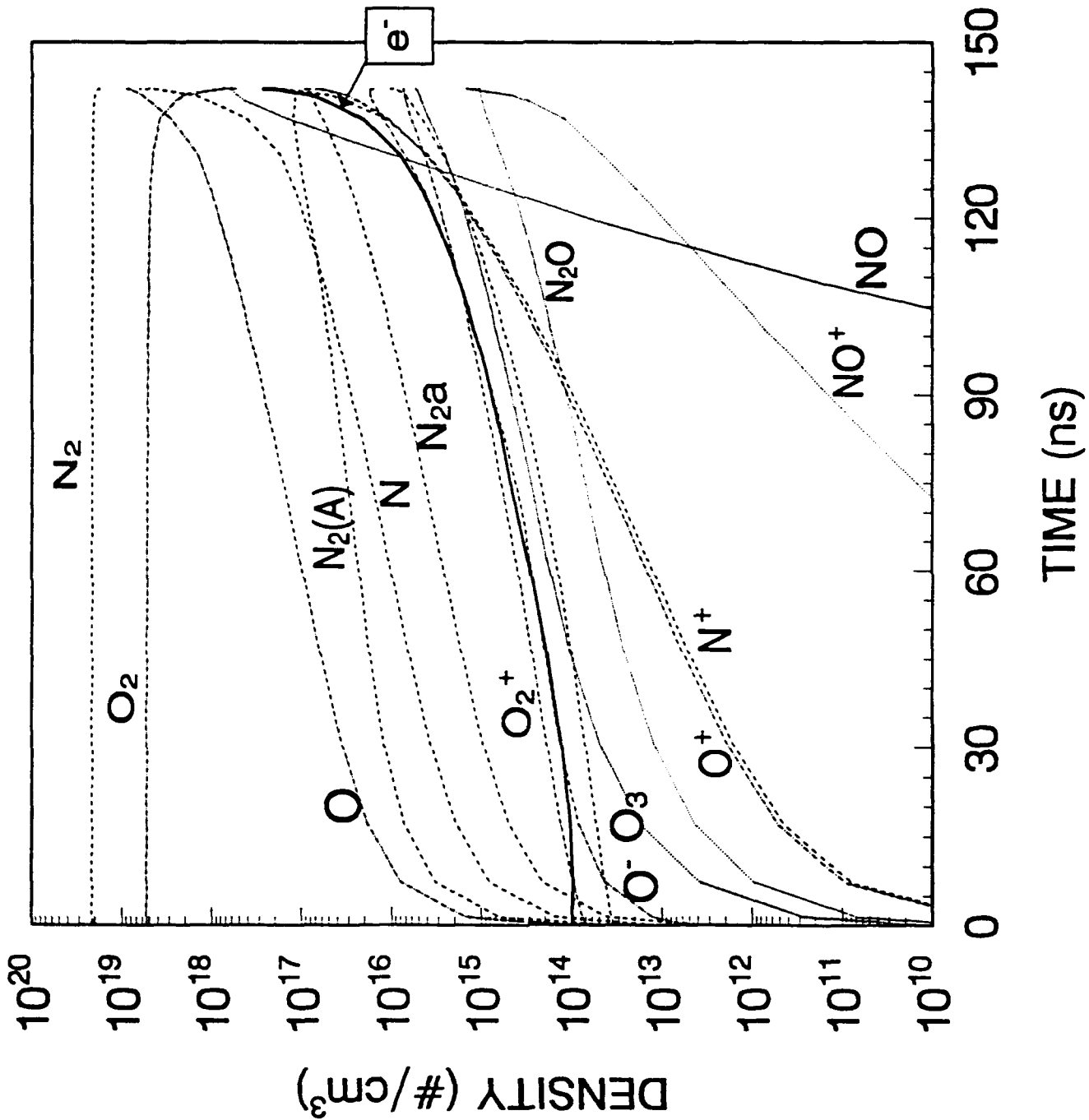


Figure 19. Populations for Nominal Air Breakdown Simulation.

VI. TOWARD A HAIRLINE APERTURE BREAKDOWN MODEL.

It appears that EMP-like radiation may cause air breakdown in hairline cracks on metallic enclosures designed to shield electronic equipment. The enhanced field in such apertures could easily exceed the DC breakdown level (3 MV/m), but the decidedly nonlinear mechanism is not well understood. The purpose of this chapter is to describe an approach to modeling such a breakdown, based on the Quasi-Equilibrium Methodology (QEM).

It is difficult to characterize the apertures accurately, because they are unintentional. However, a range of about 10 to 100 μm (10^{-5} – 10^{-4} m) is reasonable. This is smaller than the expected diameter of a filamentary streamer in a spark gap [Ref. 17, 18, and 19]. Therefore, we cannot assume a filamentary streamer provides the initial $\sim 10^{14}$ e/cm³ which triggers breakdown in a conventional (large) air gap [Ref. 2].

The scale size of interest is comparable to the expected size of a cathode fall (CF) at 1 atm, and the electron swarm is clearly not in equilibrium with the local, instantaneous electric field. A typical CF drops about 100 V across about 10 μm , for a nominal field of about 10 MV/m. One of the best non-equilibrium CF models reported in the literature is that of P. Bayle, J. Vacquie and M. Bayle [Ref. 14], which we will refer to as the BVB model. The basis of their model is the assumption that the non-equilibrium transport coefficients can be adequately approximated as the equilibrium values corresponding to the instantaneous electron temperature, which is calculated by solving the energy conservation equation. They formally assume a Maxwellian electron energy distribution function (EEDF), but that is not strictly required by their methodology. The BVB model works well because both the electron energy and transport (momentum transfer collision frequency) are dominated by the low-energy portion of the EEDF. A weakness in the BVB model is that the electron multiplication (net of gains by Townsend ionization minus losses to attachment) is dominated by the high-energy tail of the EEDF, since the ionization threshold is 12.06 eV for O₂ [Ref. 10] and 15.6 eV for N₂ [Ref. 11]. Since the high-energy tail is populated by many elastic and superelastic collisions redistributing the energy, the relaxation of the ionization coefficient may occur on a slower time scale than overall energy transfer.

The main alternatives we know of to handle these non-equilibrium phenomena are Monte Carlo methods and solution of the time-dependent Boltzmann equation. Monte Carlo methods are very robust and can be made arbitrarily accurate by using enough sample "particles", but they are computationally very expensive. Multi-temperature models have been tried with some success [Ref. 20]. These essentially amount to solving the Boltzmann equation with a crude energy-space grid. The QEM approach we prefer is based on time-dependent Boltzmann equation solutions, which are adequate as long as the local field approximation holds in a time-varying sense (or its equivalent along characteristic lines). At 1 atm, a fluid treatment is justified, avoiding the expense of "particle-pushing". The QEM approach we envision would use pre-computed Boltzmann equation solutions to characterize the relaxation time scales. An in-line time-dependent Boltzmann solution is not out of the question, but it would be quite wasteful if repeated inside the inner (non-linear) loop.

For Phase I, we did an order-of-magnitude analysis to assess the impact of the ionization rate relaxation time. (The attachment rate is not critical, because it is not as sensitive to E-field.) The conclusion reached in Chapter II is that relaxation times below 0.1 ns were too fast for non-equilibrium effects to be important. The BVB results can be used as a baseline for comparison. We need an initial electron number density, N_e , for the kinetic breakdown model. Following the BVB analysis of CO_2 , we can assume the photoemitted electrons from typical cathode materials are initially at a few eV. That corresponds to initial velocities (assuming hemispherical emission) in the regime of 10^6 m/s. If air behaves similarly to CO_2 , we can expect photoemission currents of about 10^{-7} A/cm², giving an initial electron density of about 10^8 /cm³.

A preliminary discharge kinetic analysis can be done with a nominal external circuit model. Assuming a 0.1-mm gap for 3 cm (length) and 0.3-cm depth, the micro-gap "stray" capacitance should be about 10^{-11} F (10 pF), and the stray inductance is about 3×10^{-12} H. The complete system response is difficult to assess, but a total capacitance of at least 1 nF is reasonable for typical system dimensions. An induced voltage of 1 kV across a 0.1-mm gap will produce the nominal 100 kV/cm (10 MV/m) we need for fast breakdown to occur.

Using those external circuit parameters, we ran a kinetics simulation to try to

understand the likely breakdown behavior. We used an initial 10^{10} e/cm³ for convenience. The trend is easily extrapolated back to 10^8 or any other assumed initial N_e . The surprising results are summarized in Figure 20. It shows essentially a cold Townsend avalanche, with electrons multiplying at a nearly fixed rate until the drawn current causes voltage collapse (our definition of "breakdown"). That limits the maximum electron density to about 10^{15} /cm³. More interestingly, the discharge is essentially cold, with only a few tens of degrees heating, and exhibits less complex chemistry than the transitions to full arcs modeled by Rodríguez, *et al* [Ref. 2]. This insight may lead to useful simplifications in a full micro-crack breakdown model.

However, the breakdown could be significantly enhanced by planar ionization waves. In Phase II, it is reasonable to build a 1-dimensional model of the formation phase. This 1D model would be based on solving the general current conservation equation

$$\nabla \cdot (\mathbf{J} + \dot{\mathbf{D}}) = 0$$

where $\mathbf{J} = \sigma \mathbf{E}$ is conduction current, and $\dot{\mathbf{D}} = \partial(\epsilon \mathbf{E})/\partial t$ is displacement current. In 1D, the gradient operator $\nabla \cdot (\) \rightarrow \partial(\)/\partial x$. The model should include three fluids (electrons, positive ions and negative ions) with their respective continuity equations:

$$\begin{aligned} \frac{dN_e}{dt} &= N_e(\nu_i - \nu_a) \dots \\ \frac{dN_+}{dt} &= N_e \nu_i \dots \\ \frac{dN_-}{dt} &= N_e \nu_a \dots \end{aligned}$$

The conduction current will be dominated by the more mobile electrons, so simplifications in the ion equations are justified. The general current conservation solution could obviate the need to solve one of the ion continuity equations, since the space charge ρ is given by either $\nabla \cdot (\epsilon \mathbf{E})$ or $e(N_+ - N_e - N_-)$. This has subtle numerical advantages over solving the three continuity equations first, and then

solving the E-field from Poisson's equation

$$\nabla \cdot (\epsilon E) = e (N_+ - N_e - N_-)$$

since it avoids differencing errors when $N_+ \approx N_e + N_-$ and permits numerical schemes which directly address the stiff nonlinear coupling between the E-field and the differential conductivity resulting from the high sensitivity of the Townsend ionization rate on E-field. In fact, we expect the 1D model to demonstrate the formation of either a plane ionization wave analogous to a filamentary streamer, or a non-equilibrium Townsend avalanche, depending on the applied signal.

The energy conservation equation may not be strictly necessary in the QEM formulation, but it is a simple matter to include it. Electron multiplication terms of the form $-V_e(\nu_i - \nu_a)$ or $-\langle \mathcal{E} \rangle (\nu_i - \nu_a)$ can easily be included in the continuity and energy conservation equations, respectively. Convective terms can be considered part of the total time differential, e.g.:

$$\frac{dN}{dt} \equiv \frac{\partial N}{\partial t} + \nabla \cdot (VN) = (\text{gains}) - (\text{losses})$$

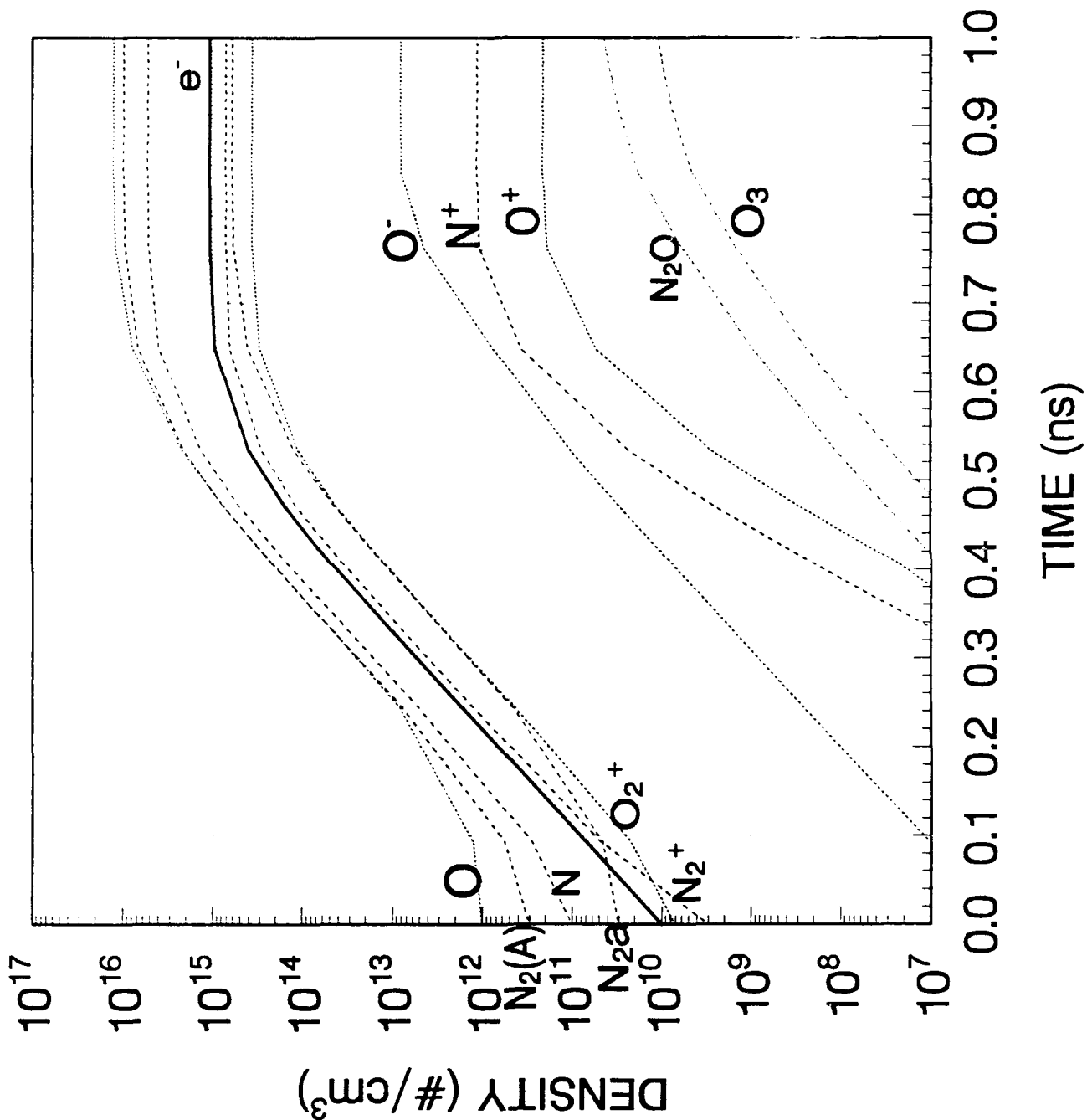
The electron pressure term $\nabla \cdot (N_e k T_e) / N_e$ can be critical if a negative glow forms, where it dominates over the E-field force.

Boundary conditions and initial conditions are straightforward. The anode can be modeled as a perfect electron absorber. The cathode is dominated by photo-emission and ion-impact emission of electrons. The emitted electron temperature is not expected to be critical, since the EEDF is quickly dominated by collisions (in the first few μm , if the BVB results are any guide). The initial conditions can be set to a background ionization level, and we let the voltage rise from zero using a realistic pulse shape.

The envisioned 1D model should yield sufficient insight into the pre-breakdown mechanisms to explain the main sources of variability in the observed breakdown behavior. It should also have quantitative predictive powers to reproduce the observable behavior of the controlled Phase II experiments. Specifically, it will model the cumulative effects between driving-signal half-cycles, such as cumulative

heating of the high-energy tail of the EEDF and the effect of that on electron multiplication. By including a simplified version of the air breakdown kinetics, the model could also follow the cumulative heating leading to thermal ionization. Thus, a single code would model the formation, heating and transition to arc phases, tracking cumulative effects through many cycles of the driving signal.

Aperture Simulation: $10^3\text{V} / 10^{-2}\text{cm}$ in Dry Air



VII. PHASE II PROGRAM PLAN.

A. PHASE II TECHNICAL OBJECTIVES.

The overall goal of the Phase II Program will be to develop a deliverable high-frequency (HF) air breakdown module applicable to micro-gaps in structures illuminated by electromagnetic pulses (EMP). That goal is supported by three objectives, and six technical tasks, each tied to a specific objective as follows:

Objective: Model Development

Task 1. Formation Phase (1-D)

Task 2. Heating Phase

Objective: Model Validation

Task 3. Marginal Effects Study

Task 4. Experimental Verification

Objective: Code Integration

Task 5. Module Documentation and Packaging

Task 6. Integrate into an EMP Coupling Code

Model development is the core of the program. The basis will be a 1-D model of a cathode fall developing into a Townsend avalanche or ionization wave. The predominantly local (almost 0-D) kinetics describing the heating phase which leads to voltage collapse (i.e. "breakdown") will be built upon the 1D model.

Model validation assures the correctness of the complete model. The final criterion is whether the model correctly predicts the behavior of empirically observable parameters, such as I/V traces or radiation output. One approach to validation is to examine neglected effects analytically, which is the purpose of Task 3. The other approach is to compare code predictions with experimental measurements, which is the purpose of Task 4.

Code integration assures the final product is usable in a real application. Task 5 embodies all actions required to transfer the module to a "user". In Task 6, we will demonstrate the use of the module in an actual EMP coupling code. We

have chosen the POLYANA code developed by BDM. Thus, this task requires participation by BDM as a subcontractor to integrate the module into the POLYANA code and test its performance. BDM will retain the final module in POLYANA for their use, but the module will remain a separate, marketable Phase III product.

B. PHASE II WORK PLAN.

Task 1. Formation Phase 1D Model.

The technical issues include the modeling of cathode-fall-like boundary conditions, formation of a Townsend avalanche and for a propagating ionization wave, AC effects, the effect of the nonequilibrium current integral, and numerical stiffness of the resulting differential equation system. Our approach is to extend Tetra's ELF1D code. ELF1D is a finite-volumes electrostatic code which solves the generalized current continuity equation:

$$\nabla \cdot (\mathbf{J} + \dot{\mathbf{D}}) = 0$$

where \mathbf{J} is conduction current ($\sigma\mathbf{E}$ in a conductivity model) and \mathbf{D} is displacement vector ($\epsilon\mathbf{E}$). The finite-volumes method has proven to be very forgiving of the shock-like front which evolves in any ionization wave [Ref. 21]. The method captures the virtual discontinuity in \mathbf{E} -field, with no errors propagating to other grid points. ELF1D is set up to handle planar, cylindrical and spherical geometries, and could be modified to model a filamentary streamer.

The model should include three charged fluids (electrons, positive ions and negative ions) with their respective continuity equations. The conduction current will be dominated by the more mobile electrons; therefore simplifications in the ion equations are justified. The general current conservation solution could obviate the need to solve one of the ion continuity equations, since the space charge ρ is given by either $\nabla \cdot (\epsilon\mathbf{E})$ or $e(N_+ - N_e - N_-)$. This has subtle numerical advantages over solving the three continuity equations first, and then solving the \mathbf{E} -field from Poisson's equation, since it avoids differencing errors when $N_+ \approx N_e + N_-$ and permits numerical schemes which directly address the stiff nonlinear coupling

between the E-field and the differential conductivity resulting from the high sensitivity of the Townsend ionization rate on E-field. We expect the 1D model to demonstrate the formation of either a plane ionization wave analogous to a filamentary streamer, or a nonequilibrium Townsend avalanche, depending on the applied signal.

The energy conservation equation may not be strictly necessary in the QEM formulation, but it is a simple matter to include it. Electron multiplication terms of the form $-V_e(\nu_i - \nu_a)$ or $-\langle \mathcal{E} \rangle (\nu_i - \nu_a)$ can easily be included in the continuity and energy conservation equations, respectively. Convective terms can be considered part of the total time differential, e.g.:

$$\frac{dN}{dt} \equiv \frac{\partial N}{\partial t} + \nabla \cdot NV = (\text{gains}) - (\text{losses})$$

The electron pressure term $\nabla \cdot (N_e T_e) / N_e$ can be critical if a negative glow forms, where it dominates over the E-field force.

Boundary conditions and initial conditions are straightforward. The anode can be modeled as a perfect electron absorber. The cathode is dominated by photoemission and ion impact emission of electrons. The emitted electron temperature is not expected to be critical, since the electron energy distribution function (EEDF) is quickly dominated by collisions, probably in the first few μm . The initial conditions can be set to a background ionization level, and we can let the voltage rise from zero using a realistic pulse shape.

Task 2. Heating Phase Model.

The Phase II 1D model should yield sufficient insight into the pre-breakdown mechanisms to explain the main sources of variability in the observed breakdown behavior. It should also have quantitative predictive powers to reproduce the observable behavior of the controlled Phase II experiments. Specifically, it will model the cumulative effects between driving-signal half-cycles, such as cumulative heating of the EEDF and the effect of that on electron multiplication. By including a simplified version of the air breakdown kinetics, the model could also follow the cumulative heating leading to thermal ionization. Thus, a single code

would model the formation, heating and transition to arc phases, tracking cumulative effects through many cycles of the driving signal.

This will be accomplished by adding a few neutrals to the kinetic set. However, since the neutrals are not moved by the E-field, this kinetic system is local (0-dimensional). The only spatial influence will be indirectly through the electron fluid. Thus, we will add a local model for few neutrals to the 3-fluid charged particles model developed in Task 1.

One issue to be explored is methods to accelerate integration of the stiff ordinary differential equation (ODE) set. One alternative is to change the independent variables to log of number densities. This should work well for integrating electrons when they avalanche, but its effect on the total ODE system needs to be explored.

Another issue to be assessed is the effect of $N_2(A)$ population on the Boltzmann analysis. As the $N_2(A)$ population increases, superelastic collisions heat the EEDF in an energy-selective manner. That increases the excitation and ionization rates. This subtle auto-feedback may change the heating phase behavior in unexpected ways.

As these technical issues are resolved, the resulting local (0-D) kinetics model will be integrated into the 1-D code. Thus, a single code will model both the formation and heating phases leading to breakdown.

Task 3. Marginal Effects Study.

By "marginal", we mean effects we expect to be negligible to first order. In this task, we will examine at least two such issues: arc formation and edge effects. After breakdown, a high-pressure discharge usually develops into an arc. On the slower time scale of arc formation ($>1\mu s$), several phenomena ignored in our breakdown model become important. Two phenomena which may also affect the breakdown are pressure buildup and radiation.

In a constricted (filamentary) arc, the high temperatures cause thermal expansion which reduces the neutral number density N , such that E/N increases for a

constant voltage. In effect, the critical voltage for electron avalanching decreases. The ohmic heating is balanced by adiabatic expansion and radiative cooling at equilibrium. For a micro-gap, we don't expect filamentary streamers to form, because the gap size is comparable to, or smaller than the expected streamer radius. Therefore, we expect expansion and radiation to be negligible to first order, but this task will confirm the adequacy of that assumption.

Even with a planar discharge, edge effects may still play a role. The field enhancements at the rough edges of a micro-gap should cause breakdown to occur at the edges before it occurs in the bulk interior. We will use simple models to determine whether such edge effects will alter the overall bulk breakdown times.

These studies will determine whether the simple 1-D model is adequate, or if thermal expansion or edge effects must be included. If necessary, we will include first-order corrections for those "marginal" effects judged to be important after all.

Task 4. Experimental Verification.

The ultimate verification of any computational model is how well its predictions match experimental observations. To this end, we will perform experiments with simplified mock-ups of micro-gaps in order to control the experimental conditions. The hardest parameter to control is the gap spacing, since in practice these are unintentional gaps. Our experimental approach is predicated on pressure scaling. By conducting the experiments at low pressures, we can scale all dimensions larger in inverse proportion to the pressure. For example, by conducting the experiments at 10^{-2} atm (7.6 Torr), we can build a gap mock-up 100 times larger than what is being modeled. As a side benefit, all time scales are slowed down by the same factor, relieving the data acquisition requirements.

Two laboratory experiments will be designed and fabricated to collect the data. One experiment utilizes a transmission line approach and the other a lumped circuit approach. The difference is that the transmission line will propagate a double-exponential electromagnetic field across the slot that will induce electric and magnetic dipoles at the slot. In the lumped circuit, the double-exponential electric field will be applied directly across the slot.

The transmission line approach is shown in Figure 21. A double-exponential voltage is produced and propagated down a transmission line to a matched load. A mismatched system can be employed to determine how oscillating currents affect the discharge characteristics of the slot. A slot is in the ground plane portion of the transmission line. The slot is thin and nearly spans the entire width of the transmission line. Data of interest include voltage across the slot, current through the slot, open-shutter photographs of the discharge, and time resolved UV measurements. The voltage and current data will provide the characteristics of voltage collapse and current growth, respectively. The closure time (time for the air to become electrically conductive) for the slot will be determined from the voltage and current waveform. Open-shutter photographs may provide information on whether the discharge is filamentary or diffuse, which affects the breakdown mechanisms involved. A temporal profile of the UV radiation emitted by the discharge will be measured. From this measurement, the electron number density can be determined. (The electron number density is an important quantity in the theoretical analysis.) Required equipment include high frequency current and voltage probes, a 500 MS/s digital storage oscilloscope (three channels preferred), open-shutter camera, UV detector circuit, power supply, circuit components (capacitors, inductors and resistors), high vacuum contact switch, copper sheet, and other miscellaneous materials.

The lumped-circuit approach is shown in Figure 22. A double-exponential voltage is simply produced across the slot. The data of interest and required equipment are the same as for the transmission-line approach except that the circuit components are different.

Experiments will be conducted down to about 10 Torr. Experimental variables and parameters include relative humidity, type of air (natural or artificial), and pressure. All materials in the vessel will be waterproof and rust-resistant. Required equipment includes an airtight vessel, roughing pump, humidity meter, thermometer, and other miscellaneous materials.

In designing the experiments, we will use computer simulations of the experimental circuits with an open circuit gap to determine the applied signals. We will produce mechanical drawings of the transmission line and the airtight vessel. The type and requirements for the sensors will be determined from results of the

circuit simulations. A test plan will be developed that details the type and volume of data needed to support the computational analysis.

After ordering the parts and materials, we will fabricate and check out the experiment. We will build the experiment and verify operation of the sensors and recording instrumentation. The collected experimental data will include the experimental parameters of pressure, relative humidity, type of air, and electric field across the slot.

We will analyze the experimental data and compare it with computational results. Here our analysis will include correlation of discharge conduction time with spatial and temporal profiles of the discharge.

Numerical simulations of the experimental conditions will be performed for direct comparison with experimental measurements. The simulations will include external circuit models matching the experimental driving circuits. Output parameters of interest include the current and voltage traces, closing times, and photodetector signal compared to computed excitation rates. Favorable comparisons will then establish confidence in the computational model.

Task 5. Module Documentation and Packaging.

In order to permit a third party user to use the resulting module, it is imperative that it be packaged in a user-friendly form. This includes documentation of the basic module itself and auxiliary programs.

During the development of the code, we will develop drivers for the module that exercises it (and perhaps sub-modules). In addition, we will also develop post-processors that read, analyze and display diagnostic data pertaining to the status of the module's internal data structure. Some of these drivers and post-processors will be useful to a user of the module, and need to be packaged accordingly.

Most importantly, a User Manual will be written for the basic module and for the drivers and post-processors. It will contain detailed instructions on how to use them, down to the level of defining each argument in the call sequence in the basic module. This is indispensable for a programmer to integrate the module

into a larger EM coupling code.

Task 6. Integrate Into An EMP Coupling Code.

The ultimate test of whether the Phase II module is usable in an EMP coupling code is to integrate it into one. Otherwise, there may be code coupling problems not obvious *a priori* which would surface only when the first real user tries to use the module. For this purpose, we have chosen the POLYANA code developed by BDM International, Inc.

BDM's POLYANA code offers a framework which is flexible, and works in the time domain. First, we will give a brief description of POLYANA then raise some issues to be addressed. Finally, we present an example of how we might address integration of the QEM module and data (I/O) handoffs. POLYANA is a time-dependent (explicit time-domain) finite difference code for solving Maxwell's curl equations in a three dimensional geometry. The code is capable of modeling complex objects by specifying the scalar conductivity and dielectric constant at each point in the problem space. Small sub-grid features such as thin wires and struts can, and have been, modeled using a built-in line integral formalism. POLYANA also has an optional air chemistry model for low altitude source region coupling. Scattered radiation is terminated at the edge of the problem space by a radiation absorbing boundary condition. The user specifies the finite difference grid, material properties, surfaces for the Huygen's sources, and sub-grid structure locations. It is written in highly transportable FORTRAN 77 which can run on a CRAY, VAX, Sun 4/110, or 386/486 class PC with an appropriate amount of RAM. POLYANA is a BDM constructed intellectual descendant of the old THRED series codes and has itself been the subject of several upgrades and/or special purpose modifications. It has been used in the past primarily for calculating the EMP coupling to a wide variety of structures including the Peacekeeper missile and the Rail Garrison system.

Initially, we propose to use a cartesian coordinate version of POLYANA rather than a conformal one for our initial effort. We can change to numerically generated coordinates later. The initial concern is timing, i.e. how fast this modified code will run a given problem with the QEM module added. Several issues need to be

resolved in order to determine how to proceed in detail, e.g.:

Do we break the problem into three pieces and use prescribed sources to connect the pieces?

If so, should the prescribed sources be consistent?

If we don't break the problem into pieces how do we want to handle the sub-grid time resolution problem in the POLYANA interface?

Specifically, how do we address the stochastic part of the problem relative to the deterministic field calculations?

Our current thinking on these issues is as follows: Self-consistency is highly desirable, and should be maintained, unless it makes the coupling burdensome. In a stand-alone mode, the QEM module would be coupled to a simple external circuit model, so currents and voltages can be solved self-consistently. Ideally, the coupled module would be structured so that the external code can model a complete aperture as a coupled network of micro-gaps or cells, each treated as a 1-D discharge independent of all the others except through the external circuit's coupling.

One simple linearization scheme is to let the external code prescribe voltage during a time step of its choosing. The QEM module would then compute current (at the end of the time step and integrated over the time step), using internal time sub-steps if needed. That way the external code time-step management is totally independent of the QEM internal time management. In practice, the need for CPU expenditure control will dictate some compromise or optional choices, perhaps patterned after the Livermore Solver of Ordinary Differential Equations (LSODE) time controls [Ref. 22].

Higher order linearization schemes are possible, based on a simple external circuit model "local" to each micro-gap cell, tied together by the external code. The nonlinear nature of the problem dictates that self-consistency be handled in an outer loop under the external code's control. A robust linearization scheme will assure fast convergence in the regime where the micro-gap is nearly linear (impedance not changing rapidly), and yet handle the fast voltage collapse and current rise which characterizes breakdown.

The stochastic part of the problem can be handled by random or pseudo-random assignments of effective gap length to the various QEM cells. Each cell will represent a small area of the aperture perimeter, over which the gap can be treated as constant. Thus, the total model will be quasi-2D or quasi-3D. The other stochastic part is the initial conditions in each gap-cell. Methods for randomizing those will be evaluated with respect to physical correctness, flexibility, ease of use, etc.

The purpose of this proposed effort is to understand how electromagnetic fields go from the outside of a structure to the inside through micro-gaps which break down. The incident EMP field is generated in the problem space outside the enclosure by a user-specified Huygen's source; then the self-consistent electromagnetic object response is computed.

Given that we have self-consistent fields at each grid cell in the problem space, let's then examine how a user would view the micro-gap. A basic assumption is that the gaps are electrically short since we are working a variant of the "classic" EMP problem (even if we use 2169 waveforms). After a random number draw is used to select which material grid cell, or cells, is to have a micro-gap, the local self-consistent electric and magnetic fields (or surface current and charge density) will be passed to the QEM subroutine to do the gap discharge calculations. POLYANA could pass those quantities to the QEM subroutine at each time-step. Then those fields could be modified to reflect the gap geometry by an approximate calculation; e.g. by using normalized De Meulnare-Von Bladel polarizabilities to calculate dipole moments and then the modified field vector components (or surface current density and charge values) prior to beginning, or continuing, the discharge calculation.

Consider the QEM handoff back to POLYANA. The QEM subroutine should pass back gap currents and voltages at each POLYANA time-step. The sub-grid line integral formalism will reconnect these quantities to the field nodes on the finite difference grid inside the macroscopic structure. We then just need to tell POLYANA where to locate our test points to obtain field information for further post processing and presentation.

Clearly, there are many issues to be resolved before the module interface can be

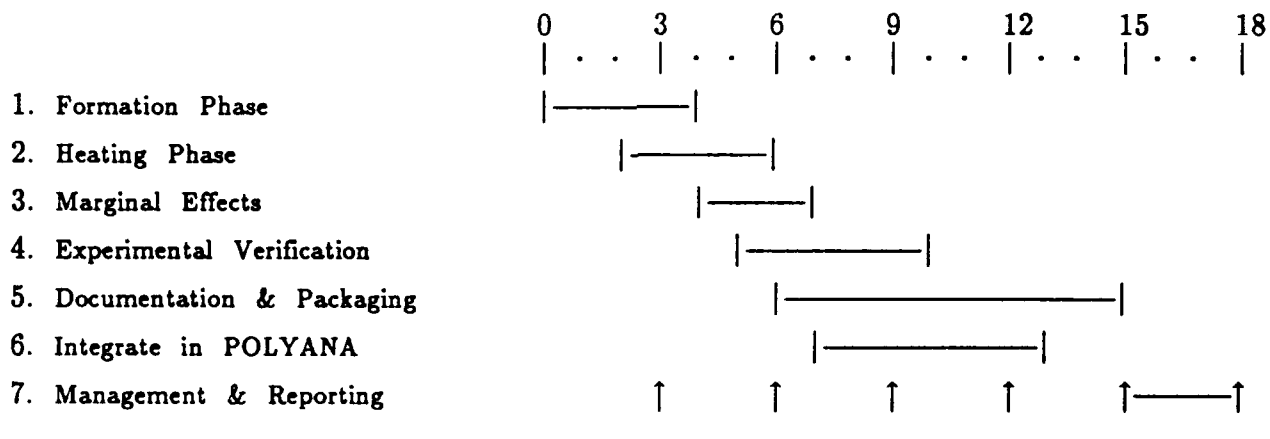
designed in detail. Actually integrating the QEM module into a real EMP coupling code like POLYANA insures that the interface issues are examined from both sides.

Finally, several test cases will be run to demonstrate the usefulness of a nonlinear micro-gap breakdown option in a full EM coupling code. The test cases will be defined jointly by Tetra and BDM in consultation with the Contract Technical Monitor, in order to insure that they are feasible, meaningful and relevant to the mission of Harry Diamond Labs.

Task 7. Management and Reporting.

Progress Reports will be submitted quarterly. A written Final Technical Report will document model derivations, results of test cases, and comparisons of experimental results with simulations. The final QEM module, drivers and post-processors, along with the Users Manual will be considered contract deliverables. One or two program reviews are recommended. A mid-term and a final presentation at Harry Diamond Labs is recommended.

Schedule (months)



Optional tasks could be defined and included in the Phase II project as pre-costed but unfunded options to the basic contract. One possibility is to extend Task 3 into development of a full 2-D breakdown model for \$50K to \$70K. Another logical extension of Task 3 would be to develop an arc phase model capable of

predicting recovery times (which relate to repetition rates). That may cost \$50 to \$60K. A logical extension of Task 5 may be to develop user-friendly driving programs using Graphic Input (GIN) and other advanced techniques as user training aids. That would cost between \$25K and \$35K. A logical extension of Task 6 is to apply the integrated POLYANA/QEM code to analyze a specific problem of vital interest to HDL. Depending on the difficulty of the specified problem, that may cost between \$25K and \$50K.

Figure 21. Transmission line experimental setup.

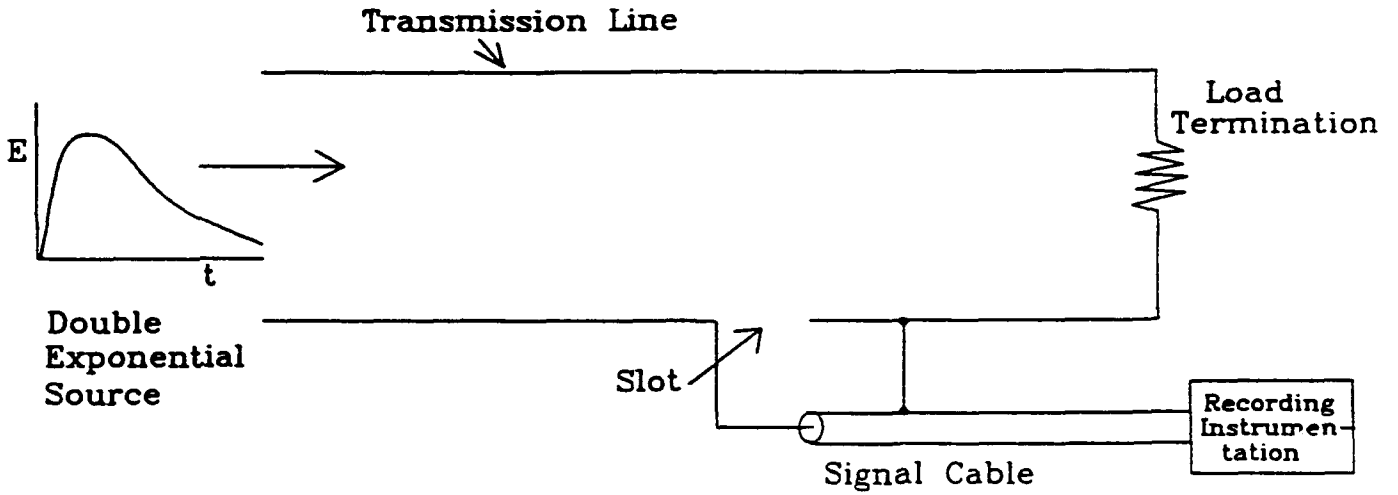
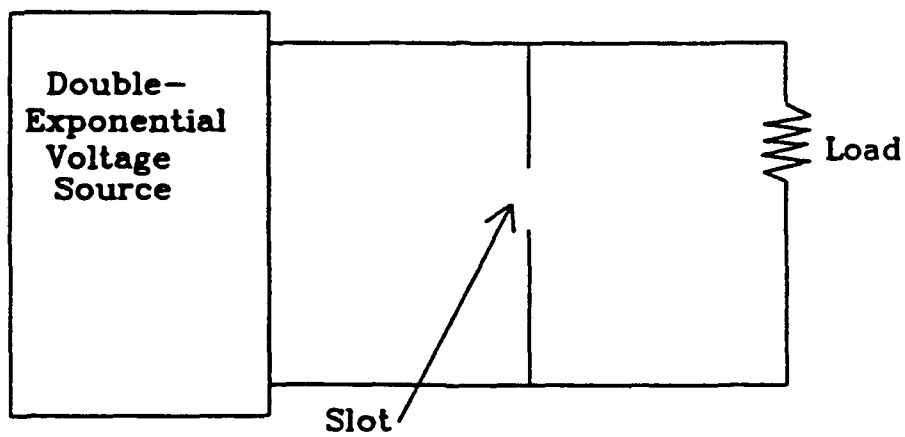


Figure 22. Lumped circuit experimental setup.



VIII. SUMMARY AND CONCLUSIONS.

In Phase I of the program, we developed the basic tools needed to build a high-frequency air breakdown model. We developed a Quasi-Equilibrium Methodology (QEM) for extending fluid electron transport models to the nonequilibrium regime. Our analysis of nonequilibrium electron transport discovered and explained a velocity overshoot effect that is not generally known. That tendency of the electrons to overshoot the equilibrium drift velocity was shown to have a profound effect on streamer behavior. We examined the extent of possible simplifications to the basic air breakdown model, concluding that factors of 2 to 5 speed-up are possible. We have identified the major phenomenological issues in a modeling strategy, and examined nonequilibrium effects on ionization waves. Finally, we presented a plan to complete development of a computational model of High Frequency air breakdown suitable for incorporation into EMP coupling codes.

Although the main application is for including nonlinear breakdown phenomena in EM coupling problems, there are other applications for a High Frequency breakdown model. The nonequilibrium effects on ionization waves can be very important. An accurate ionization wave model will find applications in arc lamp and spark gap design [Ref. 16], the study of HV vacuum insulator surface flashover [Ref. 23], and perhaps in advanced concepts using controlled ionization waves to accelerate non-relativistic ion beams [Ref. 24]. It also seems to have applications in modeling of air avalanche switches for EMP generation [Ref. 25], and the velocity overshoot described in Chapter II has been observed in solid state devices [Ref. 26]. The QEM applied to other gases may also find application in low pressure glow discharge switches, such as the Cs-vapor tacitron [Ref. 27]. However, in order to limit the scope, the focus of the Phase II effort will be to model micro-gap breakdown in apertures of shielding structures illuminated by EMP.

The final product will be a computational module incorporating the air breakdown model, which can be either run in a stand-alone configuration, or incorporated into a larger EMP coupling code. To demonstrate the usefulness of the module, we will indeed integrate it into the POLYANA EMP coupling code developed by BDM. Tetra plans to market the module separately in Phase III, not only to the EMP community, but also to the community designing and developing glow

discharge switches, lasers and arc lamps, as we have successfully done with our Electric Field Analysis (tetraELFTM) codes in which the complete range of marketing activities were conducted. This included market research, market analysis, development of descriptive materials and specification sheets, all followed by an international sales campaign.

As a direct result of the Phase I accomplishments of the Quasi-Equilibrium Model of HF Air Breakdown project, we are in a position to develop in Phase II a breakdown model to predict breakdown in apertures illuminated by EMP. Such a computational model, once fully verified, would have applications in arc lamp and spark gap design, including switches for EMP generation, vacuum HV insulators, solid-state devices, and probably others we have not discovered.

For approximately \$300K, HDL would obtain what very well could become the standard computational model for assessing the effect of air breakdown on the response of electronic systems to EMP and other high-power electromagnetic threats. Our plans to commercially market the computational module in Phase III would make this modeling capability accessible to the EMP community and those in other application areas.

References

1. Rodríguez, A. E., "Externally Generated EMP Threats to Satellites - Final Technical Report", Tetra Corporation, July 1985.
2. Rodríguez, A. E., Morgan, W. L., Touryan, K. J., Moeny, W. M., and Martin, T. H., "An Air Breakdown Kinetic Model," J. Appl. Phys., Vol. 70, No. 4, p. 2015, August 15, 1991.
3. Martin, T. H., "An Empirical Formula for Gas Switch Breakdown Delay," pp. 73-79, Digest of Technical Papers, 7th IEEE Pulsed Power Conference, Monterey, CA, June 11-14, 1989.
4. Longley, H. J., Longmire, C. L., "Electron Mobility and Attachment Rate in Moist Air," MRC-N-222, Dec 1975.
5. Cobine, J.D., Gaseous Conductors, Dover, New York, 1958.
6. Francis, G., Ionization Phenomena in Gases, Butterworths, London, 1960.
7. Ivanchenko, A. I, and Shepelenko, A. A., Teplofiz. Vys. Temp. 20, 636, 1982.
8. Morgan, W.L. and Penetrante, B., "ELENDF77: A Time-Dependent Boltzmann Solver for Partially Ionized Plasmas," Computer Physics Communications 58, 127, 1990.
9. Phelps, A. V. and Pitchford, L. C., Joint Institute for Laboratory Astrophysics (JILA) Report 26, 1985.
10. Phelps, A. V., JILA Rpt 28, 1985.
11. Kieffer, L. J., JILA Rpt 13, 1973.
12. Hayashi, M., "Electron Collision Cross-Section Molecules Determined from Beam and Swarm Data," Swarm Studies and Inelastic Electron-Molecule Collisions, ed. L. C. Pitchford, et al., Springer-Verlag, NY, 1987.
13. Kunkardt, E. E., Webber Research Institute, Polytech University, Farmingdale, NY, private comm., May 1991.
14. Bayle, P., Vaquie, J. and Bayle, M., Phys Rev A, 34(1), 360-371 and 372-380, July 1986.
15. Morrow, R., "Theory of Positive Corona in SF₆ Due to a Voltage Impulse", IEEE Trans. Plasma Sci. 19(2), 86-94, April 1991.

16. Rodríguez, A. E., Touryan, K. J., Moeny, W. M., Morgan, W. L., "Laser Triggered Spark Gap Modeling Final Report," SAND91-7065, August, 1990.
17. Wells, J., "Electrical Breakdown of Trigatron Gas Switches Operating in Air", UNM MS Thesis EE, 1987, T. Martin, advisor.
18. Wu, C. and Kunhardt, E. E., Phys Rev A, 37(11), 4396, June 1988.
19. Rodríguez, A. E., Touryan, K. J., and Moeny, W. M., "Resolution Requirements for Modeling Streamer Formation in a Spark Gap", 1989 IEEE Conference on Plasma Science, May 22-24, 1989, Buffalo, NY.
20. Pitchford, L. C., and Phelps, A. V., "Multi-Term Boltzmann Analysis of Electrons in N₂," JILA Final Report, 1 Oct 79 - 30 Sep 80, AFWAL Contract MIPR-FY1455-80-00608.
21. Morrow, R., "Properties of Streamers and Streamer Channels in SF₆," Phys. Rev. A, 3(3), 2233, 1989.
22. Hindmarsh, A. C., "ODEPACK, A Systematized Collection of ODE Solvers," Scientific Computing, ed. R. S. Stepleman, et al., North Holland, Amsterdam, pp. 55-64, 1983.
23. Gray, E., "Vacuum Surface Flashover: A High-Pressure Phenomenon," J. Appl. Phys. 58(1), 1 July 1985.
24. Rodríguez, A. E. "A Preliminary Ion Surfatron Feasibility Analysis: A White Paper," submitted to AFWL, May, 1991.
25. Mayhill, D. J., Yee, J. H, and Villa, F., "Computational and Experimental Progress on Laser-Activated Gas Avalanche Switches for Broadband, High-Power Electromagnetic Pulse Generation," submitted to SPIE International Symposium, Boston, MA, September, 1990.
26. Chen, D., Kan, E. C., and Ravaioli, U., "An Analytical Formulation of the Length Coefficient for the Augmented Drift-Diffusion Model Including Velocity Overshoot," Electron Devices, 38(6), p. 1484, June 1991.
27. El-Genk, M. S., Murray, C., Chaudhuri, S., "Experimental Evaluation of Cs-Ba Thermionic Switch/Inverter - 'Tacitron'," 1991 IEEE Conference, August 4-9, 1991, Boston, MA.

Appendix A

Relaxation to a Sliding Quasi-Equilibrium — An Algorithm

The purpose of this Appendix is to document the derivation of an algorithm for integrating the elementary differential equations on which the Quasi-Equilibrium Methodology (QEM) is based. The basis of the QEM model is that the collision frequencies and rates relax toward values in equilibrium with the local electric field not instantaneously, but with certain characteristic lag times.

Consider electron velocity as an illustration. The momentum conservation equation without convective terms reduces to an electron fluid acceleration equation:

$$\dot{V} = \frac{e}{m} E - V \nu$$

(V is electron fluid velocity, e/m is charge to mass ratio, and E is the driving electric field.) Under Local Field Approximation (LFA) methods, the collision frequency ν driving the friction-like loss term is considered a function of local, instantaneous E -field (usually pre-tabulated from empirical measurements or Boltzmann solutions). The QEM approach varies in that ν is calculated as the solution of an accompanying Ordinary Differential Equation (ODE):

$$\dot{\nu} = (\nu - \nu_q) / \tau$$

where the equilibrium solution ν_q and characteristic time τ are considered functions of instantaneous E .

Electron number density, with a source term S and attachment loss rate α , is governed by an ODE of similar form:

$$\dot{N}_e = S - N_e \alpha$$

We may generalize the ODE form by calling the dependent variable Y , the driving function S , and the loss/collision rate R , thus:

$$\dot{Y} = S - Y R \quad \text{and} \quad \dot{R} = (R - R_q) / \tau$$

where R_q is the equilibrium value R tends toward with a relaxation time τ .

Consider a discrete time step Δt such that the driving functions S , R_q and τ are well-behaved enough to use linear interpolation. If R_q and τ were constant, the second equation would have an exact solution

$$R(t) = R_q + (R_0 - R_q) \exp(-t/\tau)$$

where $R_0 \equiv R(0)$ is the initial value. This is the essential relaxation behavior: the instantaneous difference from the equilibrium solution decays exponentially in time.

A graphical interpretation of the ODE is that the slope of the R vs t curve must point at each instant toward the tip of an arrow at the equilibrium value R_q

delayed by one time constant τ . If both are changing in time, the system is "chasing" a moving target. A linear interpolation of the "target" represents a "Sliding Quasi-Equilibrium", such as the long-dashed line in Figure 1 labelled "SQE". Decay of the initial difference from that SQE represents a "Relaxation to a Sliding Quasi-Equilibrium" (RSQE). If the initial and final equilibrium R-values are R_0 and R_1 , then the targets at 0 and Δt are easily estimated by linear interpolation. Let's designate them R_0' and R_1' . Thus, the RSQE algorithm is:

$$R_n \equiv R(\Delta t) = R_1' + (R_0 - R_0') e^{-\int (1/\tau) dt}$$

Since we have chosen Δt such that τ is well-behaved, the integral can be evaluated by linear averaging:

$$\int (1/\tau) dt \approx \langle \Delta t / \tau \rangle$$

where the angular brackets $\langle \rangle$ stand for the operation of taking the linear average over Δt .

In Figure 1, the function $R(t)$ was calculated at 32 sub-steps of Δt , and the more accurate 32-step solution is plotted along with the one-step solution curve. Notice they are nearly indistinguishable.

The same procedure could then be applied to the primary ODE, with the initial/final values:

$$Y_0 = S_0/R_0 \quad \text{and} \quad Y_1 = S_1/R_n$$

However, the driving function $R(t)$ is not linear. The integral

$$\int R dt = \langle R_s \rangle \Delta t + (R_0 - R_0') \tau (1 - e^{-\langle \Delta t / \tau \rangle})$$

where $\langle R_s \rangle = 0.5(R_0' + R_1')$ is the linear average SQE R-value, is accurate to the same order as $R(\Delta t)$. Using linear interpolation to define SQE target values Y_0' and Y_1' as illustrated in Figure 2, we would calculate the solution as:

$$Y(\Delta t) \approx Y_1' + (Y_0 - Y_0') e^{-\int R dt}$$

Notice the one-step function (the curve labeled "RSQE" in Figure 2) overestimates $Y(t)$ compared to the more accurate 32-step solution. The reason is that the true SQE target depends on an $R(t)$ function which is not linear. By the time we get near Δt , R has relaxed to much nearer the R_1 equilibrium value than implied by a linear interpolation. It is important that the RSQE solution not be less accurate than an equilibrium solution for large $\Delta t \gg 1/R$.

A next-order correction is needed to account for the nonlinear shape of the Y-function SQE. For a short characteristic time $1/R \ll \Delta t$, it is reasonable to back up to $t' = \Delta t - 1/R$, with the expectation that the forward projection $t' + 1/R(t')$ will be close to Δt , and thus a better basis for estimating Y_1' at Δt . Since the analytic function $R(t)$ is known, we can calculate

$$Y'(t') = S(t')/R(t')$$

where $S(t')$ is calculated by linear interpolation. This is the basis for a nonlinear SQE Y -function target. However, for stability, we must use a form for t' which does not result in a backward projection ($t' < 0$). Defining $R_{ave} = \int R dt / \Delta t$, the form $t' = \Delta t \exp(-1/\int R dt)$ tends to 0 for $1/R_{ave} \gg \Delta t$, and tends asymptotically to $\Delta t - 1/R_{ave}$ for $1/R_{ave} \ll \Delta t$. That is the form used in the computations displayed in Figure 3. Notice that the modified RSQE one-step solution is indistinguishable from the more accurate 32-step solution near the beginning and near the end of the test case time step, but an error is evident in-between. (Keep in mind that the test case is intentionally stressful.)

The source of the error is that the simple linear SQE was being used for the extrapolation to 0 of Y_0' . For consistency, we ought to use the same Y', Y_1 data pair to re-compute Y_0' . That amounts to using a near-implicit tangent to the non-linear SQE as the basis for the Y -relaxation algorithm. It makes the algorithm more implicit, by weighting data near the end of the time step heavier as the characteristic time $1/R_{ave}$ becomes small compared to Δt . With that modification, the "implicit" RSQE algorithm gave the results shown in Figure 4. Notice the agreement is excellent at all times.

However, that does not guarantee the 1-step integral of Y is acceptably accurate. Within the RSQE formalism, the integral is calculated as:

$$\int Y dt \approx \Delta t \left[\langle Y_s \rangle + \Delta Y_0 \left[\frac{1 - e^{-\int R dt}}{\int R dt} \right] \right]$$

where $\langle Y_s \rangle$ is the average of the intercepts Y_0' and Y_1' , ΔY_0 is the initial difference to the intercept ($Y_0 - Y_0'$). The problem with that algorithm is illustrated well by a test case designed to accentuate the tendency of $Y(t)$ to overshoot its eventual equilibrium value. The test case uses initial values $Y_0 = 0$, and $R_0 = 1$, tending toward a constant equilibrium value $R_q = 5$ in a constant relaxation time $\tau = 10$, with a constant source term $S = 5$. The solution Y vs t curve is shown in Figure 5.

The simple "linear" RSQE algorithm seriously over-estimates the integral, but the non-linear algorithm using the "implicit" offset t' near $\Delta t - 1/R_{ave}$ under-estimates it. The reason is that a tangent to the nonlinear SQE near the end of the time step extrapolated back to $t = 0$ misses the peak. An alternate algorithm using a more "explicit" displaced time t' near $1/R_0$ over-estimates the integral, but not as badly as the linear algorithm. A new approach is needed.

We decided to estimate the "dominant" time t_d at which we should expect

$$Y(t_d) \Delta t \approx \int Y dt$$

Substituting the RSQE algorithm expressions, we get

$$Y_s + \Delta Y_0 e^{-R t_d} \approx \langle Y_s \rangle + \Delta Y_0 \left[\frac{1 - e^{-\int R dt}}{\int R dt} \right]$$

where Y_s and $\langle Y_s \rangle$ are respectively the instantaneous and average SQE values. Assuming $Y_s(t_d) \approx \langle Y_s \rangle$,

$$t_d \approx -\ln\left[\frac{1-e^{-\int R dt}}{\int R dt}\right] / R_0$$

where we used the explicit time constant $1/R_0$ outside the bracket, to insure that the peak region is given adequate weight. As shown in Figure 6, the resulting solution for the test case is nearly indistinguishable from the "correct" 32-step calculation (dashed line). Notice all the algorithms are good at small times, but the rejected algorithms have errors which grow with time.

In conclusion, an algorithm has been developed to integrate the ODE pair

$$\dot{Y} = S - Y R \quad \text{and} \quad \dot{R} = (R - R_q)/\tau$$

by a method we call Relaxation to a Sliding Quasi-Equilibrium. It has the correct asymptotic behavior for time steps Δt much smaller than or much greater than the dominant characteristic times, and behaves well anywhere in-between. The ODE characteristic times τ and $1/R$ may well be much smaller than the characteristic time Δt on which the driving functions S , R_q and τ change. The RSQE algorithm applies even for $\Delta t \gg 1/R$, a situation which is too stiff for conventional numerical integration methods. (For example, if $R \Delta t \approx 10^2$, a "brute force" algorithm would need 10^4 substeps for a 1% tolerance.) Furthermore, RSQE time steps can be chosen by the more liberal criterion of limiting changes in the slopes of driving functions, rather than the more restrictive criterion of limiting changes in the functions themselves.

In the long run, the RSQE algorithm is not merely more efficient; it may be the only feasible method to handle the strong stiffness introduced by the Quasi-Equilibrium Methodology.

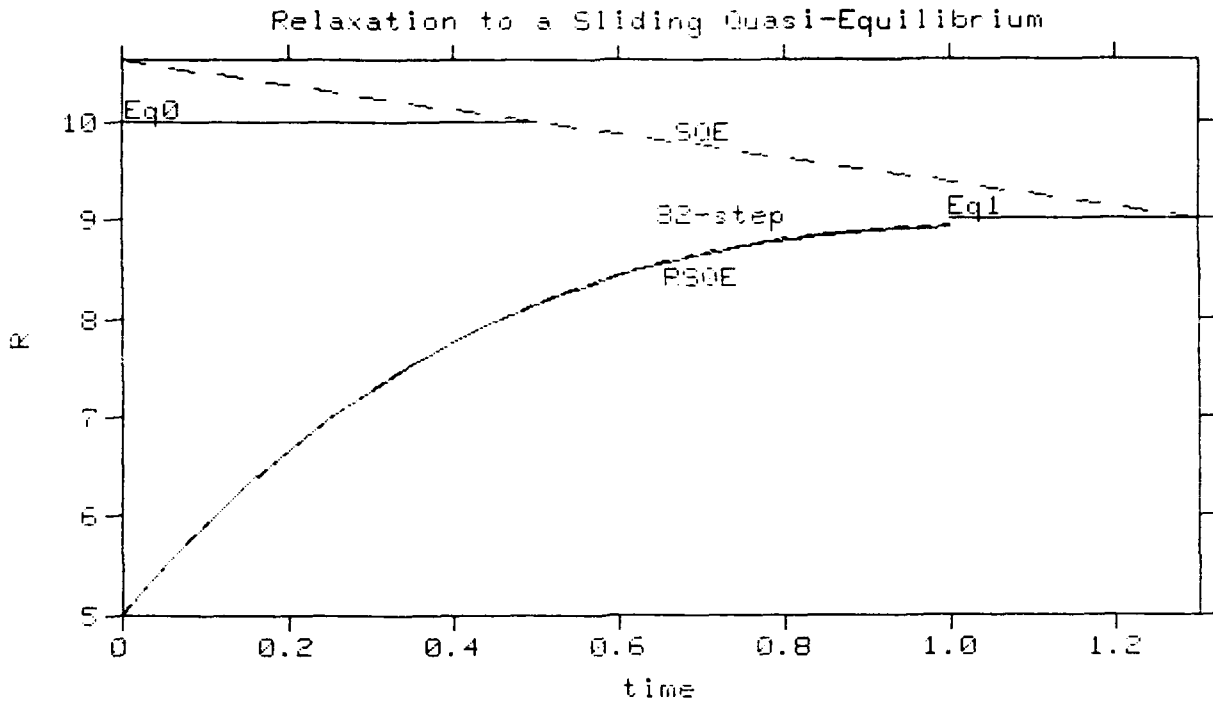


Figure 1. Linear RSQE solution to secondary ODE $\dot{R} = (R-R_q)/\tau$

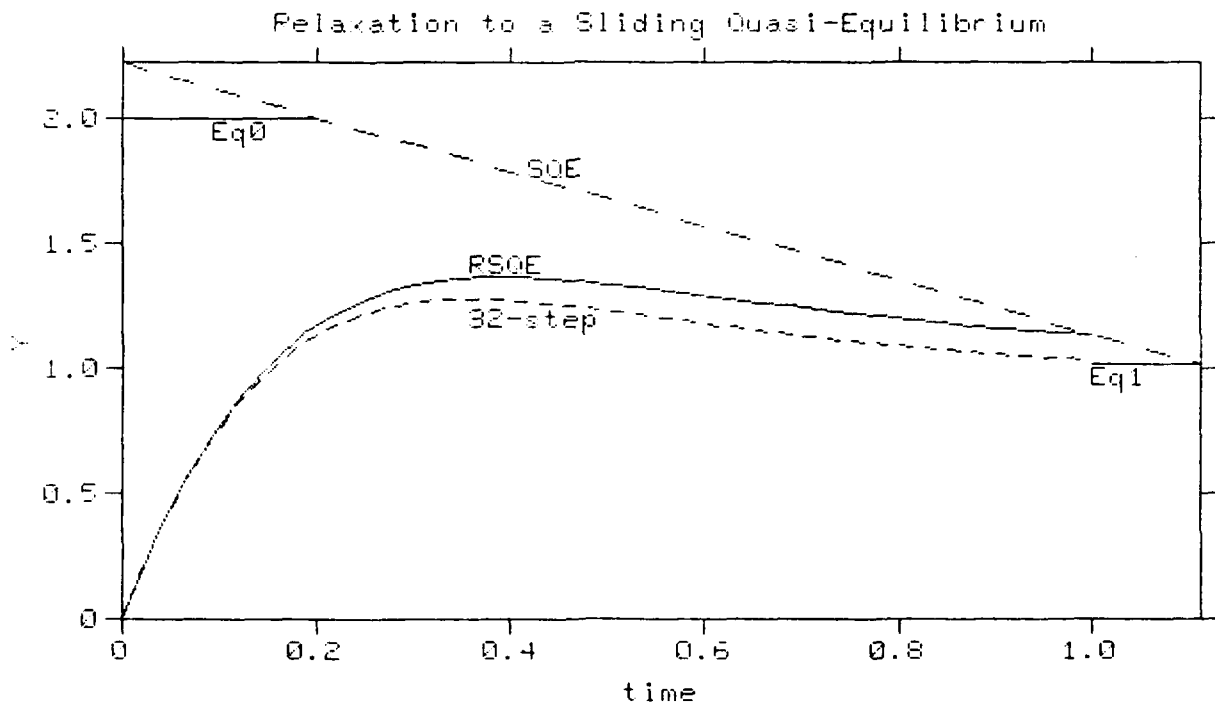


Figure 2. Linear RSQE solution to primary ODE $\dot{Y} = S - Y R$

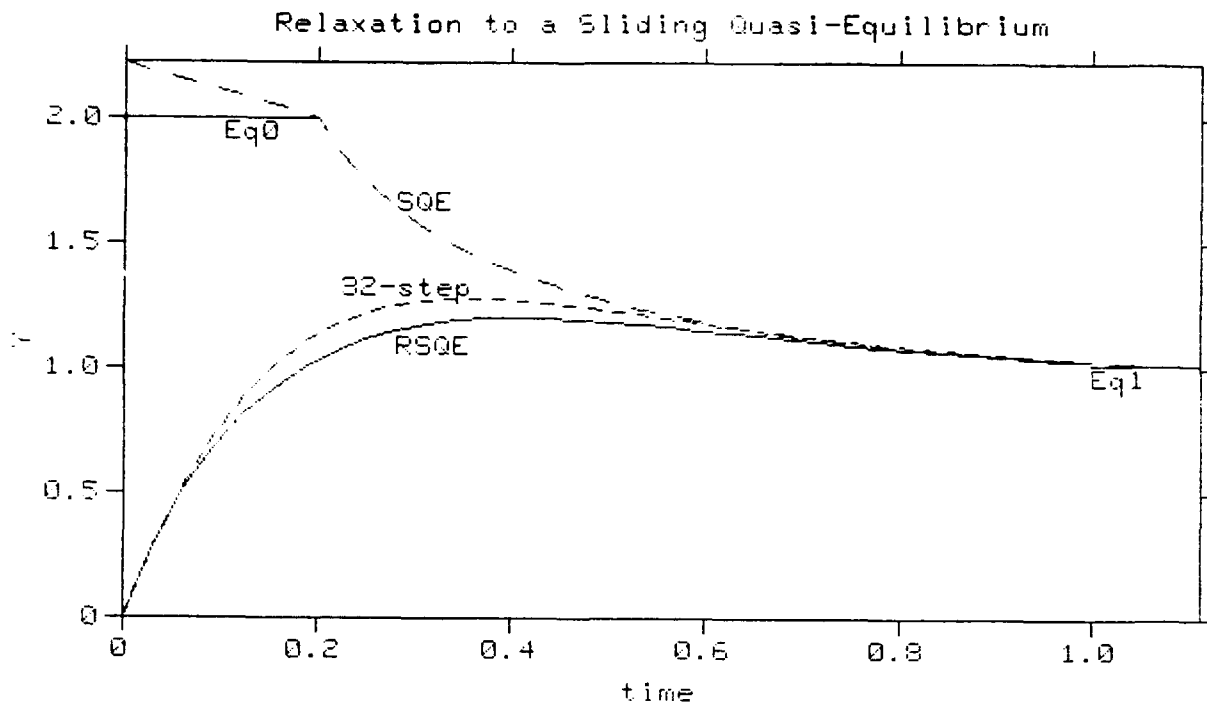


Figure 3. Nonlinear RSQE solution to primary ODE $\dot{Y} = S - Y R$

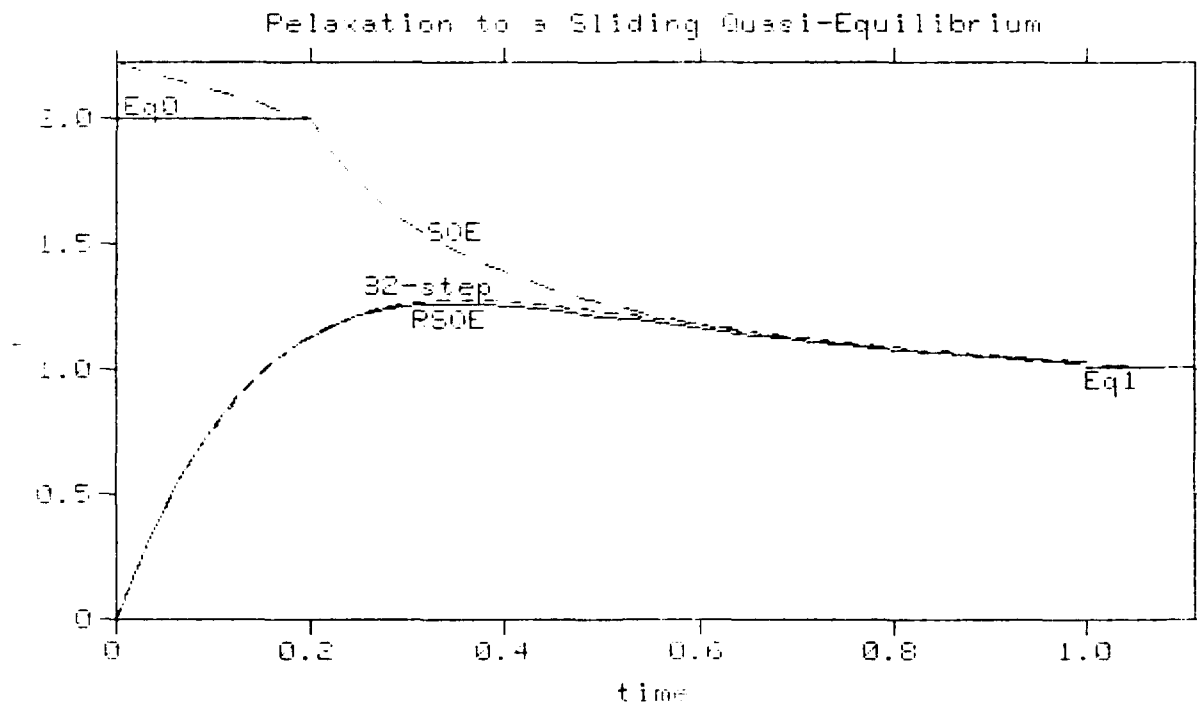


Figure 4. Implicit RSQE solution to primary ODE $\dot{Y} = S - Y R$

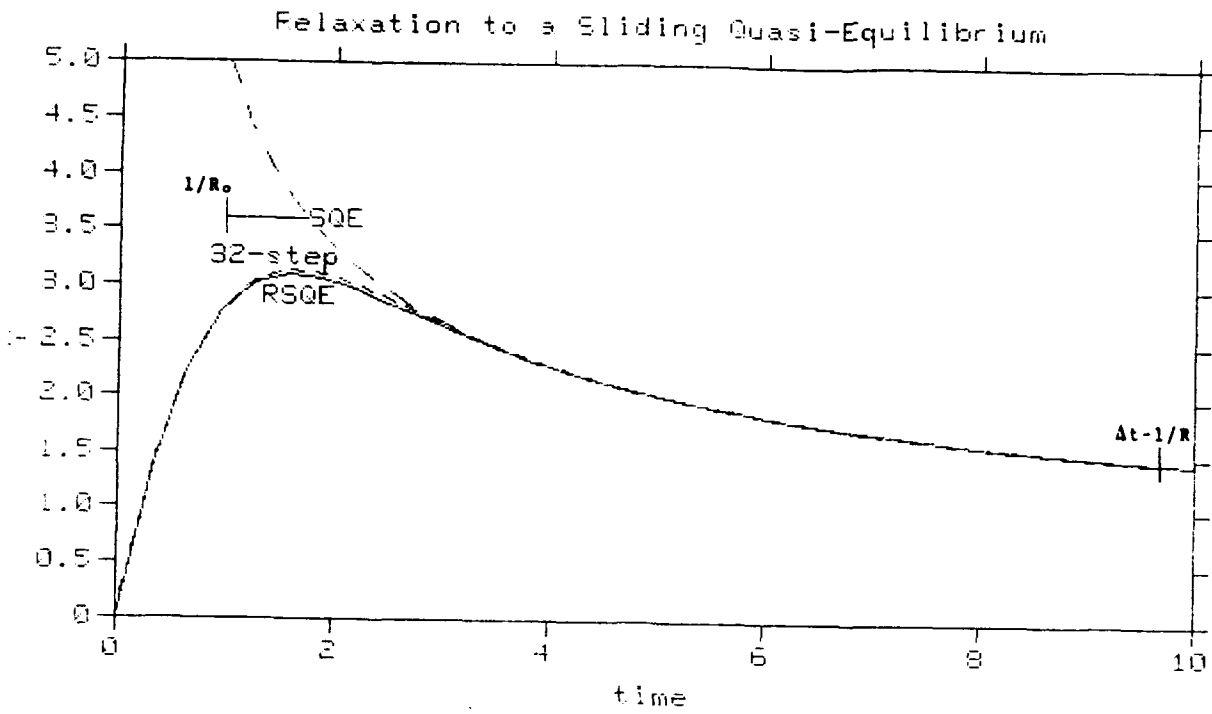


Figure 5. Y-solution for test case $S=5$, $R_q=5$, $\tau=10$.

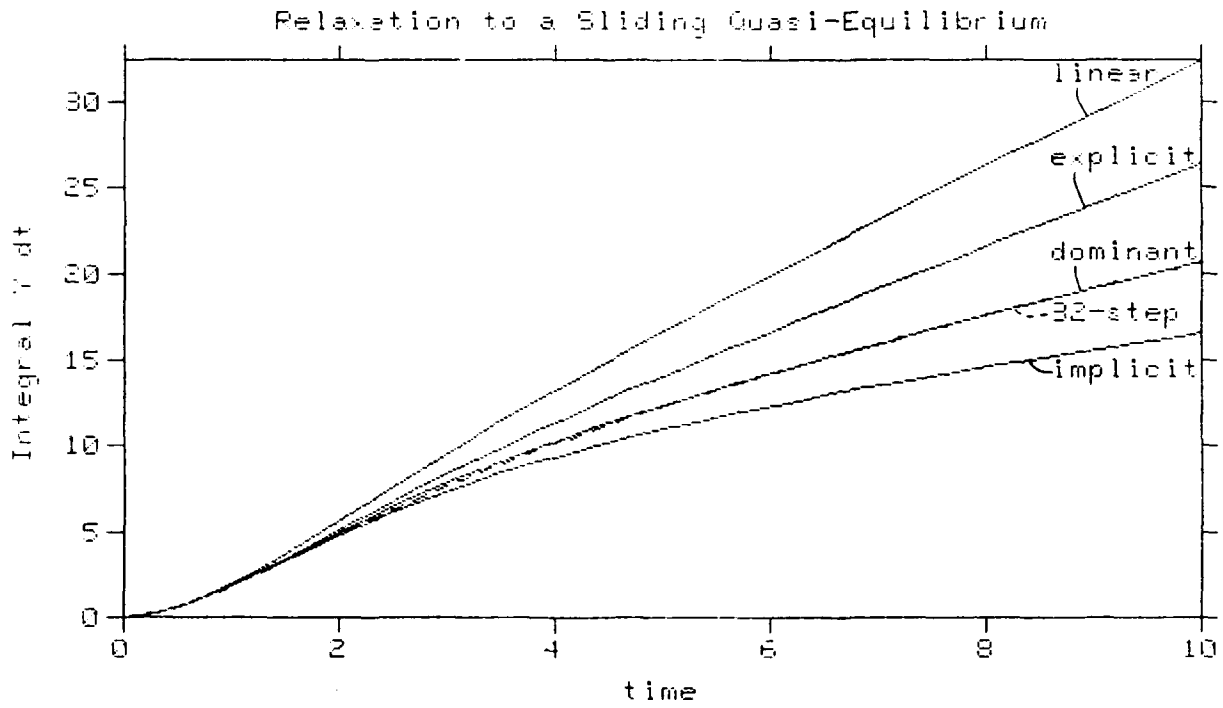


Figure 6. $\int Y dt$ by different algorithms.

Appendix B

Assessment of the Importance of Particulates in the Propagation of High Pressure Streamers

Mark J. Kushner
Dept. of Electrical & Computational Engineering
University of Illinois
Champaign-Urbana, IL 61801-2991

Industrial environments, at least outside of clean rooms, are contaminated by airborne particulates and particulates on most surfaces. Airborne particulates, whether they are dielectrics or conductors, are capable of acquiring and sustaining an electrical charge. In this respect, particulates can often be active components of plasmas sustained in ambient air.

Large ungrounded particles in plasmas (sizes commensurate to the Debye length) will most often negatively charge in the same fashion that a floating surface in contact with a plasma will negatively charge to balance the flux of electrons and ions to its surface. In this respect, particulates resemble massively large, multiply charge negative ions. Particles having sizes of a few microns will have 100s to 1000s of elementary charges on their surfaces.

The fact that particles are suspended in the plasma (either electrostatically or buoyantly) and are negatively charged detrimentally impacts the plasma. The consequences of particulate contamination of plasmas are at least four-fold. First, the electron energy distribution (EED) of a contaminated plasma is shifted to lower energies compared to the EED in a pristine plasma at the same E/N (electric field/number density) (Ref. 1). Second, due to their effective large momentum transfer cross sections, particulates will channel current in the plasma out of regions of high contamination into regions of low contamination (Ref. 2). Third, particles are large recombination centers for electrons and ions which can significantly affect the balance between electron production and electron loss. Fourth, during transient operation, the number of electrons required to charge a particle may be a non-negligible fraction of the total charge available.

To determine whether particles must be considered during the development and propagation of streamers, the following scaling laws should be considered.

1. Assume that the streamer is propagating into an otherwise nonionized gas which is contaminated by particles having density N and radius R . Further assume that the path length of propagation is ℓ . A streamer will certainly encounter these uncharged particles if the fractional area density exceeds unity. That is, particulate contamination is important for these conditions if

$$4\pi R^2 N \ell > 1.$$

2. If the streamer is propagating into an ionized plasma, the critical radius increases to approximately $R + \lambda$, where λ is the Debye length. [$\lambda = 750 \times (T_e/n_e)^{\frac{1}{2}}$ cm, T_e = electron temperature (eV), n_e = electron density (cm^{-3})].

3. The charge required to raise the potential of a spherical dielectric having radius R to V volts is $V \cdot 4\pi\epsilon_0 \cdot R$. The rate of charging is approximately $j \cdot A$, where j is the current density and A is the cross sectional area of the particle. Assuming the particle will charge to a few times the electron temperature, the charging time is

$$\Delta t = 2.5 \cdot \epsilon_0 \cdot T_e / (j \cdot R)$$

4. The effective rate of recombination of electrons and ions on the surface of a particle is given by the flux of ions to its surface, since all ions will neutralize once they strike the negative charge. The effective rate coefficient for recombination is therefore given by the cross sectional area of the particle and the ion thermal velocity,

$$k_r = v_{ion}(\pi R^2) \text{ cm}^3\text{s}^{-1}$$

The total rate of recombination is $\nu_r = k_r \cdot N$, and can exceed 10^3 s^{-1} in moderately hot and contaminated plasmas.

(NOTE: These expressions must be evaluated for the conditions of a particular problem.)

In previous studies of the effects of particles in low pressure glow discharges, it was determined that the operating E/N of the discharge increased with increasing particle contamination because the rate coefficients for ionization decreased (Ref. 1 and 2). In the 0.1 - 10 Torr range, significant effects were found for particulate densities (radius 1 μm) exceeding 10^3 cm^{-3} . In general, the threshold for this effect increased with increasing pressure and increasing E/N . As a practical consideration, in inhomogeneously contaminated plasmas this may not be a particularly important effect. This apparent contradiction results from the fact that once the particles charge, the current will be channeled away from heavily contaminated regions into less contaminated regions. Hence, the local lowering of the ionization rate coefficients may not be particularly important. In high pressure plasmas where the local field approximation is valid ($p > 10\text{s} - 100 \text{ Torr}$) and the Debye length is short (μm 's) the isolation of the particles by these mechanisms is fairly efficient.

The fact that current is constricted into less contaminated regions will have secondary effects. For example, in electronegative plasmas where the attaching species is consumed (e.g., excimer lasers) the constriction described above causes a nonuniform consumption of the attaching gas and may cause an operating point instability (Ref. 3). This effect alone can cause arcing and streamers. There may also be a measurable secondary effect on the self-sustaining E/N because a plasma which is constricted into a smaller region has a higher resistance.

References

1. McCaughey, M. J., and Kushner, M. J., "Electron Transport in Dusty Argon Plasmas," Appl. Phys. Lett. 55, 951 (1989).
2. McCaughey, M. J., and Kushner, M. J., "A Model for Particulate Contaminated Glow Discharges," J. Appl. Phys., 69, 6952 (1991).
3. Kushner, M. J., "Microarcs as a Termination Mechanism of Optical Pulses in Electric Discharge Excited KrF Lasers," Trans. Plasma Science, 19, 387 (1991).